iScience

CellPress
OPEN ACCESS

Article

Identification of metabolic pathways underlying FGF1 and CHIR99021-mediated cardioprotection

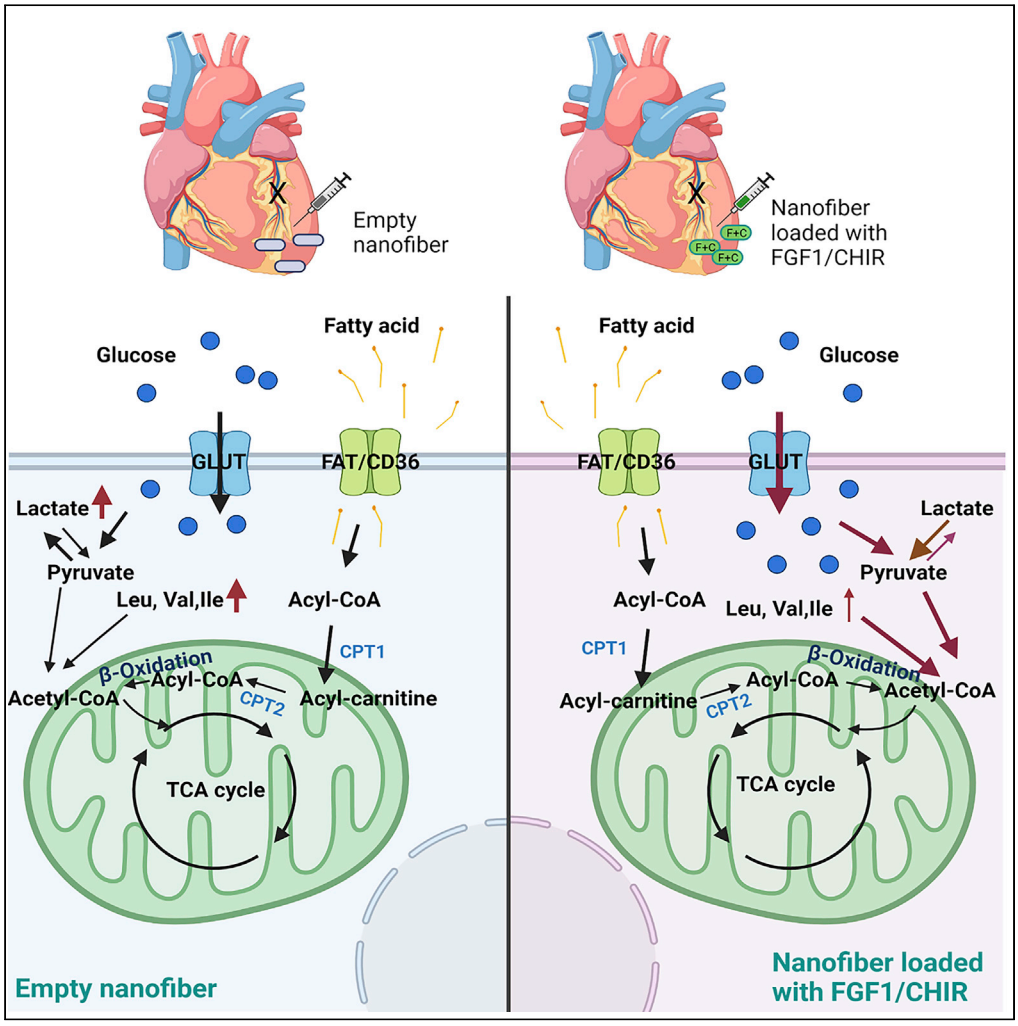

Bing Xu, Fan Li, Wenjing Zhang, ..., Jingwei Xie, Haiwei Gu, Wuqiang Zhu

hgu@fiu.edu (H.G.)
zhu.wuqiang@mayo.edu (W.Z.)

Highlights

FGF1/CHIR confer cardioprotection in myocardial infarction animals

FGF1/CHIR enhance the capability of ischemic hearts to produce energy via glycolysis

FGF1/CHIR reduce the abundance of branched chain amino acids in ischemic hearts

This study reveals a novel approach to correct metabolic disorders in ischemic hearts

Xu et al., iScience *25*, 104447
June 17, 2022 © 2022 The Author(s).
https://doi.org/10.1016/j.isci.2022.104447

iScience

CellPress
OPEN ACCESS

Article

Identification of metabolic pathways underlying FGF1 and CHIR99021-mediated cardioprotection

Bing Xu,[1,2,8] Fan Li,[1,3,8] Wenjing Zhang,[4,5] Yajuan Su,[6] Ling Tang,[1] Pengsheng Li,[1] Jyotsna Joshi,[1] Aaron Yang,[1] Dong Li,[1] Zhao Wang,[7] Shu Wang,[5] Jingwei Xie,[6] Haiwei Gu,[4,5,*] and Wuqiang Zhu[1,9,*]

SUMMARY

Acute myocardial infarction is a leading cause of death worldwide. We have previously identified two cardioprotective molecules — FGF1 and CHIR99021— that confer cardioprotection in mouse and pig models of acute myocardial infarction. Here, we aimed to determine if improved myocardial metabolism contributes to this cardioprotection. Nanofibers loaded with FGF1 and CHIR99021 were intramyocardially injected to ischemic myocardium of adult mice immediately following surgically induced myocardial infarction. Animals were euthanized 3 and 7 days later. Our data suggested that FGF1/CHIR99021 nanofibers enhanced the heart's capacity to utilize glycolysis as an energy source and reduced the accumulation of branched-chain amino acids in ischemic myocardium. The impact of FGF1/CHIR99021 on metabolism was more obvious in the first three days post myocardial infarction. Taken together, these findings suggest that FGF1/CHIR99021 protects the heart against ischemic injury via improving myocardial metabolism which may be exploited for treatment of acute myocardial infarction in humans.

INTRODUCTION

Ischemic heart disease is a leading cause of mortality globally accounting for more than nine million deaths a year (Nowbar et al., 2019). Adult mammalian cardiomyocytes permanently exit the cell cycle and lose regeneration capacity. Loss of myocardium because of injuries, such as acute myocardial infarction (MI), often results in fibrotic scar and depressed cardiac function. Infarct size is a major determinant of prognosis in these patients (Heusch, 2020). Despite the success of interventional coronary procedures to restore coronary blood perfusion, morbidity and mortality from acute MI are still significant. Developing cardioprotective strategies to reduce infarct size is important for treating ischemic heart disease. Preclinical studies have shown that ischemic preconditioning or pharmacological agents provide significant cardioprotection (Heusch, 2020). However, clinical studies have reported inconsistent results (Baxter et al., 2000; Bulluck et al., 2016). Several drugs that have shown cardioprotection in preclinical trials, such as cyclosporine A, KAI-9803 (a selective δ-protein kinase C inhibitor peptide), and MTP131 (a cytochrome c peroxidase inhibitor), failed to elicit consistent cardioprotective effects in patients with myocardial infarction (Heusch, 2020; Botker et al., 2020). Therefore, new cardioprotective approaches are required to treat ischemic heart disease.

It has been reported that impaired metabolism and energy supply contributes to the development and progression of heart failure, and metabolism correction represents a promising approach in treating patients with heart failure (Stanley et al., 2005; Brown et al., 2017). In the mammalian heart, cardiomyocyte metabolism undergoes a transition from anaerobic glycolysis to oxidative phosphorylation during development (Kolwicz et al., 2013; Lopaschuk and Jaswal, 2010). Glucose metabolism yields pyruvate, which is then converted to acetyl-CoA in mitochondria and enters the tricarboxylic acid (TCA) cycle. Oxidation of glucose and fatty acids produces reduced equivalents nicotinamide adenine dinucleotide (NADH) and Flavin adenine dinucleotide ($FADH_2$). The electron transport chain in mitochondrial inner membrane accepts electrons from these NADH and $FADH_2$ and transforms them into ATP. This process is called oxidative phosphorylation (OXPHOS), responsible for over 90% of ATP in the aerobic heart, whereas the rest of ATP is produced by glycolysis (Lopaschuk et al., 1994). In mammals, pyruvate can be converted to lactate in cytosol and vice versa, and this reaction is catalyzed by lactate dehydrogenase (LDH) (Cluntun et al., 2021;

[1]Department of Cardiovascular Diseases, Physiology and Biomedical Engineering, Center for Regenerative Medicine, Mayo Clinic Arizona, 13400 E Shea Blvd, Scottsdale, AZ, USA 85259

[2]Department of Cardiology, Northern Jiangsu People's Hospital, Clinical Medical College, Yangzhou University, Yangzhou 225001, China

[3]Department of Kinesiology, South China Normal University, Guangzhou 510631, China

[4]Center for Translational Science, Department of Cellular Biology and Pharmacology, Herbert Wertheim College of Medicine, Florida International University, Port St. Lucie, FL 34987, USA

[5]College of Health Solutions, Arizona State University, Phoenix, AZ 85287, USA

[6]Department of Surgery, University of Nebraska Medical Center, Omaha, NE 68198, USA

[7]Department of Diabetes and Cancer Metabolism, Beckman Research Institute, City of Hope National Medical Center, Duarte, CA 91010, USA

[8]These authors contributed equally

[9]Lead contact

*Correspondence: hgu@fiu.edu (H.G.), zhu.wuqiang@mayo.edu (W.Z.)

https://doi.org/10.1016/j.isci.2022.104447

This is an open access article under the CC BY-NC-ND license (http://creativecommons.org/licenses/by-nc-nd/4.0/).

Hui et al., 2017). Lactate can be an important energy source for the myocardium and its level is maintained in a balanced manner in healthy hearts (Bergman et al., 2009). Energy metabolism of cardiomyocytes in the ischemic myocardium switches from mitochondrial OXPHOS to glycolysis and lactic fermentation (Karwi et al., 2018; Honkoop et al., 2019). Increased intracellular lactate may inhibit glycolysis, which further impairs ATP production in a vicious cycle (Leite et al., 2011).

Fibroblast growth factor 1 (FGF1) plays important roles in various biological processes such as embryonic development, wound healing, neurogenesis, and angiogenesis (Powers et al., 2000). FGF1 is also associated with nutrient sensing, glycemic control, and insulin sensitization (Suh et al., 2015). Intravenous administration of FGF1 at the beginning of reperfusion protects the heart from ischemic injury (Huang et al., 2017; Gasser et al., 2017; Sancar et al., 2022). In addition, cardiac specific overexpression of FGF1 enhances cardiac function recovery and attenuates myocardial necrosis induced by acute ischemia and reperfusion (Palmen et al., 2004). Moreover, myocardial ischemia causes hyperglycemia and insulin resistance (Yang et al., 2019; Wang et al., 2015). Treatment with FGF1 increases insulin-dependent glucose uptake in skeletal muscle, inhibits glucose production in liver, and improves systemic insulin sensitization in diabetic mice (Suh et al., 2014). FGF1 does so by upregulating GLUT4 expression and translocation to plasma membrane in skeletal muscle in an insulin-independent manner (Ying et al., 2021). A recent report also suggests that FGF1-FGFR1 signaling pathway regulates blood glucose level by inhibiting lipolysis and hepatic glucose production (Sancar et al., 2022).

CHIR99021 is a GSK3β antagonist/Wnt agonist (Linseman et al., 2004; Watcharasit et al., 2008). GSK-3β is a serine/threonine kinase originally identified as a molecule that regulates glycogen metabolism through phosphorylation and downregulation of glycogen synthase (Rylatt et al., 1980). GSK-3β is also involved in a wide range of cellular processes including the regulation of multiple transcription factors, the Wnt pathway, nuclear factor κB, endoplasmic reticulum stress, embryogenesis, apoptosis and cell survival, cell cycle progression, and cell migration (Forde and Dale, 2007). Inhibition of GSK3β reduces reperfusion injury and necrosis by inhibiting the opening of MPTP (mitochondrial permeability transition pore) and cell death. MPTP is a nonspecific channel in the inner membrane of mitochondria. Under normal physiological conditions, MPTP is turned off. During ischemia-reperfusion, MTPT is turned on and mitochondrial membrane potential is lost, leading to leakage of apoptotic and necrotic proteins from mitochondria to the cytoplasm, eventually apoptosis or necrosis (Miura and Tanno, 2010; Juhaszova et al., 2009; Ahmad et al., 2019). In isolated cardiomyocytes, knockdown of GSK3β using siRNA led to an increased MPTP opening threshold (Ghaderi et al., 2017). GSK3β also has been shown to activate p53 (Watcharasit et al., 2003) and inhibit HIF1α (Mottet et al., 2003). Using pharmacological or genetic approach to stabilize HIF-1α protects the heart against acute ischemia-reperfusion injury by promoting aerobic glycolysis, decreasing mitochondrial oxidative stress, activating hexokinase 2 (HK2), and inhibiting MPTP opening (Ong et al., 2014). Besides, inhibition of GSK-3β activity has also been shown to protect neuronal cells against rotenone-induced cell death by inducing HK2, leading to enhanced glycolysis and metabolism (Gimenez-Cassina et al., 2009).

We have recently discovered that the combination of FGF1 and CHIR99021, but not individually, confers cardioprotection against acute MI-induced heart failure in the mouse and porcine models. Specifically, we found that nanoparticles carrying both FGF1 and CHIR99021 have a sustained release profile and improve heart function in post-MI mice and pigs via preventing cardiomyocyte death and increasing neo-vasculogenesis (Fan et al., 2020a). Despite the pro-angiogenic function of FGF1/CHIR99021, cardiomyocyte death typically takes place within an hour in ischemic myocardium, which is likely earlier than formation of new vessels in the heart (Hausenloy and Yellon, 2013). Therefore, we hypothesize that other mechanisms may contribute to FGF1/CHIR99021-mediated early cardioprotection.

In this study, we aimed to investigate whether a combination of FGF1 and CHIR99021 alters myocardial metabolic pathways that have been shown to have cardioprotective effects in myocardial infarction. Nanofibers formulated with FGF1 and CHIR99021 were intramyocardially injected to the infarction area immediately after MI induction. At day 3 and 7 after surgery and nanofiber treatment, hearts were harvested for mass spectrometry-based metabolomics assays and Western blotting. MI leads to increased glycolysis, decreased glucose and fatty acid oxidation, and impaired branched-chain amino acid (BCAA) degradation. Treatment of FGF1/CHIR99021 promotes glucose catabolism flux including glycolysis and glucose oxidation, and BCAA degradation in post-MI hearts. Thus, our study discovered a new cardioprotective therapeutic against acute MI injuries via modulating cardiac metabolism.

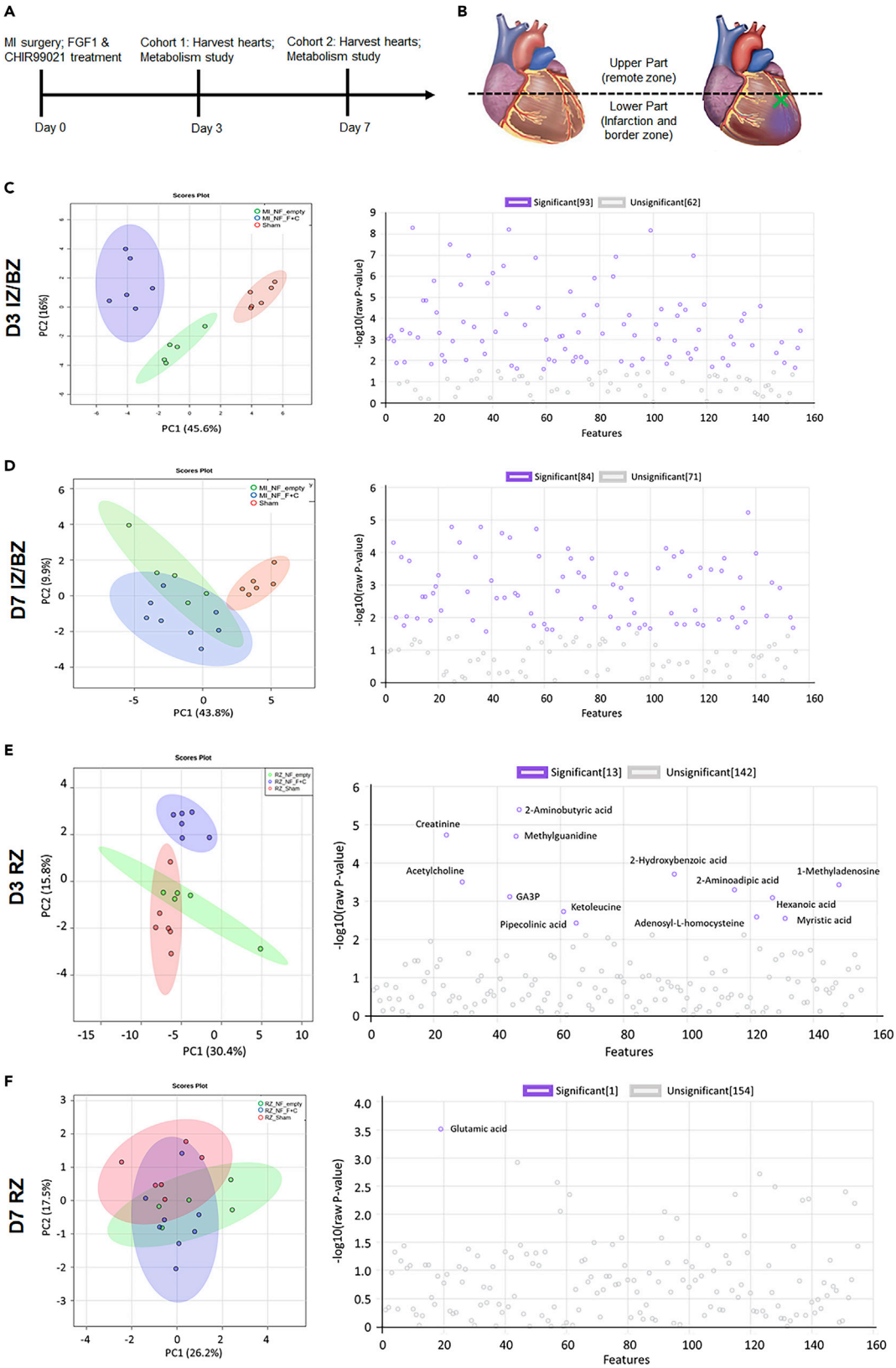
A
MI surgery; FGF1 & CHIR99021 treatment
Cohort 1: Harvest hearts; Metabolism study
Cohort 2: Harvest hearts; Metabolism study
Day 0
Day 3
Day 7
B
Upper Part (remote zone)
Lower Part (Infarction and border zone)
C
D3 IZ/BZ
Scores Plot
MI_NF_empty
MI_NF_F+C
Sham
PC1 (45.6%)
PC2 (16%)
Significant[93]
Unsignificant[62]
-log10(raw P-value)
Features
D
D7 IZ/BZ
PC1 (43.8%)
PC2 (9.9%)
Significant[84]
Unsignificant[71]
E
D3 RZ
RZ_NF_empty
RZ_NF_F+C
RZ_Sham
PC1 (30.4%)
PC2 (15.8%)
Significant[13]
Unsignificant[142]
Creatinine
2-Aminobutyric acid
Methylguanidine
Acetylcholine
2-Hydroxybenzoic acid
2-Aminoadipic acid
1-Methyladenosine
GA3P
Ketoleucine
Hexanoic acid
Pipecolinic acid
Adenosyl-L-homocysteine
Myristic acid
F
D7 RZ
PC1 (26.2%)
PC2 (17.5%)
Significant[1]
Unsignificant[154]
Glutamic acid

Figure 1. Metabolic characterization of myocardium at 3- and 7-days post-MI

MI and sham-operated mice were treated with intramyocardial injections of NF_empty (without FGF1 and CHIR99021) or NF_F + C (with FGF1 and CHIR99021). Hearts were collected at day 3 and day 7 post-MI for metabolic study.

(A) Experimental design for animal surgery and NF treatment.

(B) Strategy to collect heart samples from infarction/border zones (IZ/BZ) vs. remote zone (RZ).

(C and D) PCA and scatter diagram of metabolites in IZ/BZ myocardium at 3- and 7-days post-MI.

(E and F) PCA and scatter diagram of metabolites from RZ myocardium at 3- and 7-days post-MI. In panel C and (E) sham (n = 6), MI_NF_empty (n = 5), MI_NF_F + C (n = 6). In panel D and F, sham (n = 6), MI_NF_empty (n = 5), MI_NF_F + C (n = 8). One-way ANOVA with Fisher's least significant difference test. $p<0.05$ were considered as significant.

RESULTS

Impact of FGF1/CHIR99021 on myocardial metabolism after MI

Myocardial infarction was surgically induced via permanent ligation of left anterior descending (LAD) coronary artery. PLGA nanofiber segments formulated with FGF1 and CHIR99021 were intramyocardially injected to three sites in the infarct area immediately after LAD ligation (Figure 1A). The samples from infarction and border zones (IZ/BZ, lower part of left ventricle) (Figure 1B) were collected for LC-MS/MS assay at day 3 (D3) and day 7 (D7) after MI. Heatmap of abundance of metabolites from heart samples showed differentially regulated metabolites [Figures S1A and S1B; Table S1 "Metabolites at IZ/BZ, related to Figure 1"]. Principal component analysis (PCA) revealed a clear separation of metabolomic profile in the myocardium of sham and post-MI animals at day 3 post-MI after receiving NF_empty or NF_F + C (Figure 1C). Among the 155 metabolites reliably detected, 93 showed significant changes ($p < 0.05$) in at least one of the group comparisons (sham vs. MI and NF_empty, sham vs. MI and NF_F + C, and MI and NF_empty vs. MI and NF_F + C) as shown in the scatter plot. At day 7 post-MI, distinct metabolic profiles in the hearts of sham vs. MI animals were shown in PCA analysis, whereas the metabolic profiles in the two groups of MI animals were similar (Figure 1D). Among the 155 metabolites reliably detected, 84 showed significant changes ($p < 0.05$) in at least one of the three group comparisons as shown in the scatter diagram.

We also analyzed the metabolomic data collected using the samples from the remote zone (RZ, upper part of left ventricle) (Figures 1E and 1F). Heatmap of abundance of metabolites at 3 and 7 days after MI showed the differentially regulated metabolites [Figures S2A and S2B, Table S2 "Metabolites at RZ, related to Figure 1"]. As shown in PCA analysis, the metabolic profile in the remote zone of post-MI hearts receiving NF_F + C was similar to the hearts from sham animals. Only 13 metabolites showed significant changes ($p < 0.05$) in at least one of the group comparisons (sham vs. MI and NF_empty, sham vs. MI and NF_F + C, and MI and NF_empty vs. MI and NF_F + C) as shown in scatter diaphragm (Figure 1E). At day 7 post-MI, the metabolic profiles in the remote zone of the three groups of animals were similar and only one out of the 155 metabolites detected showed significant change in the three group comparisons (Figure 1F).

FGF1/CHIR99021 enhances glycolysis in ischemic myocardium

Glycolysis is a metabolic pathway that converts glucose in the cytoplasm to pyruvate, which produces adenosine triphosphate (ATP) in an anaerobic manner. Metabolite analysis showed that 3 or 7 days of MI increased metabolite abundance in the glycolytic pathway, including glucose, glucose 6-phosphate, and glycogenolysis/glycogenesis (glucose 1-phosphate) (also possibly from galactose) (Figure 2A). These metabolic changes were further amplified by FGF1/CHIR99021 at day 3 instead of day 7 (Figure 2A). The abundance of metabolites in the mannose metabolism pathway (mannose and mannose 6-phosphate) was significantly higher in the hearts of post-MI animals receiving NF_F + C compared with sham or post-MI animals receiving NF_empty (Figure 2A). At day 7, the MI group still had higher mannose 6-phosphate, but not mannose, and FGF1/CHIR99021 had no effect on mannose or mannose 6-phosphate. Mannose can be phosphorylated by hexokinase to produce mannose-6-phosphate, which is converted to fructose-6-phosphate by phosphomannose-isomerase and then enters the glycolysis pathway (Pitkanen et al., 2004). Taken together, these data indicate an increased glycolysis flux in the mouse hearts 3 and 7 days post-MI, and FGF1/CHIR99021 further augmented glycolysis only at day 3 but not at day 7 post-MI.

Glycolysis is regulated by a series of enzymes. To confirm the metabolomic data and further understand how FGF1/CHIR99021 regulates glycolysis, we performed Western blotting to determine the expression of rate-limiting enzymes of glycolysis (Figure 2B). Hexokinase (HK) catalyzes the conversion of glucose to

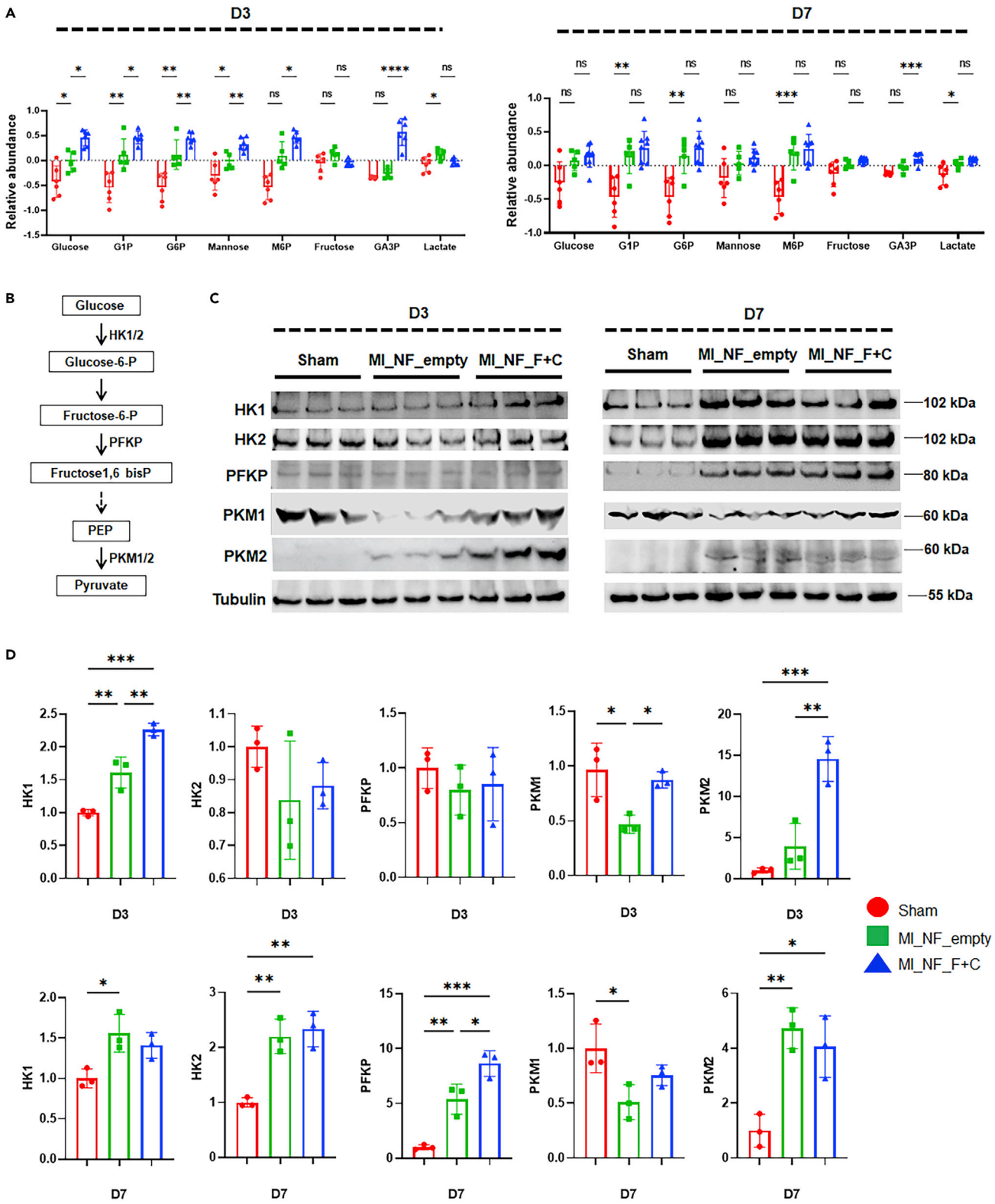

Figure 2. Impact of FGF1/CHIR99021 on glucose metabolism in ischemic myocardium

Post-MI mice received intramyocardial injections of NF_empty or NF_F + C. Hearts were collected at day 3 and day 7 post-MI.

(A) Abundance of metabolites in the pathways of carbohydrate metabolism in infarction zone/border zone (IZ/BZ) myocardium at day 3 and day 7 post-MI.

Figure 2. *Continued*

(B) Diagram of glycolysis pathway.

(C) Myocardial tissues from sham and post-MI mice (IZ/BZ) were collected for Western blot analysis with antibodies against HK1, HK2, PFKP, PKM1 and PKM2.

(D) Densitometric signal quantitation of band intensity for HK1, HK2, PFKP, PKM1 and PKM2. Data were normalized to tubulin. In panel A, for day 3, sham (n = 6), MI_NF_empty (n = 5), MI_NF_F + C (n = 6); for day 7, sham (n = 6), MI_NF_empty (n = 5), MI_NF_F + C (n = 8). In panels C and D, n = 3 per group. Data in panel A, C and D are represented as mean+/−SD. *p < 0.05, **p < 0.01, ***p < 0.001, one-way ANOVA with Tukey's Honestly Significant Difference Test.

glucose-6-phosphate. There are four isoforms of HKs with HK1 and HK2 being the most abundant ones. HK1 is widely expressed in almost all mammalian tissue, whereas HK2 is mainly expressed in insulin-sensitive tissues such as heart, skeletal muscle, and adipose tissue (Lowry and Passonneau, 1964; Purich and Fromm, 1971; Mandarino et al., 1995; Nederlof et al., 2014). Our data showed that HK1 was induced by MI at day 3 and day 7 post-MI, which was further increased by the treatment of FGF1/CHIR99021 at day 3. HK2 was also increased by MI at day 7 but treatment of FGF1/CHIR99021 had no additional effect (Figures 2C and 2D). Phosphofructokinase-1 platelet-type (PFKP) is an isoform of PFK which expresses in various cell types (Kahn et al., 1979; Fernandes et al., 2020; Dunaway, 1983). PFKP catalyzes the conversion of fructose 6-phosphate to fructose 1, 6-phosphate. Our data showed that PFKP was not affected by MI or treatment of FGF1/CHIR99021 at day 3; however, it was induced by MI and the treatment of FGF1/HIR99021 at day 7 (Figures 2C-2D). Pyruvate kinase catalyzes the last step of glycolysis by converting phosphoenolpyruvate to pyruvate. There are two isoforms in the muscle (PKM1 and PKM2) (Israelsen and Vander Heiden, 2015). It was recently reported that MI inhibits expression of PKM1 and induces expression PKM2 in mouse hearts (Magadum et al., 2020). In consistent these observations, our data showed that expression of PKM1 was reduced and expression of PKM2 was increased at day 3 and 7 post-MI. Treatment of FGF1/CHIR99021 further increased the expression of PKM2 in ischemic myocardium at day 3 (Figures 2C-2D). Taken together, these data indicate an increased glycolysis in ischemic myocardium, and treatment of FGF1/CHIR99021 enhances the capacity of ischemic myocardium to utilize glycolysis as energy source.

FGF1/CHIR99021 increases pyruvate oxidation in ischemic myocardium

The increased activity of glycolysis is usually associated with increased lactate in tissues (Bergman et al., 2009). Our data showed that the abundance of lactate was indeed increased by MI. However, it was normalized by the treatment of FGF1/CHIR99021 (Figure 2A). Intracellular lactic acid can be produced from pyruvate in the last step of glycolysis which is a reversibly catalyzed by LDH (Liu et al., 2018) or be obtained from peripheral circulation by monocarboxylic acid cotransporters (Halestrap et al., 1997; McCullagh et al., 1997). LDHs are homotetramers or heterotetramers assembled from two different subunits (M and H), which are encoded by two separate genes, LDHA (M) and LDHB (H), respectively (Zdralevic et al., 2017). LDH1 is composed of four LDHB subunits and catalyzes the conversion from lactate to pyruvate, and LDH5 is composed of four LDHA subunits and drives the conversion from pyruvate to lactate (Figure 3) (Fritz, 1965). Expression of LDHA is induced during physiological (e.g., running and swimming) and pathological (e.g., pressure overload induced by thoracic aortic constriction) cardiac hypertrophy (York et al., 1976; Dai et al., 2020). We performed Western blotting experiments to check the expression of LDHA and LDHB in post-MI mouse hearts. Our data showed that LDHA was decreased and LDHB was increased in the mice receiving NF_F + C compared with the sham or MI mice receiving NF_empty at day 3 post-MI. And these changes were normalized at day 7 post-MI (Figures 3B and 3C). These data suggest that treatment of FGF1/CHIR99021 may reduce the conversion of pyruvate to lactate, and/or increase the conversion of lactic acid to pyruvate in the ischemic myocardium at the first 3 days post-MI, thus preventing the accumulation of lactic acid.

We further assessed the expression of pyruvate dehydrogenase (PDH), one of the three enzymes that comprise the pyruvate dehydrogenase complex (PDC). PDC catalyzes the conversion of pyruvate and CoA into acetyl-CoA (Figure 3D). PDH in the MI_NF_empty group was significantly reduced at day 3 and day 7 post-MI compared with the sham group. However, NF_F + C partially rescued the inhibition of PDH induced by ischemia (Figures 3E and 3F). These data indicate that treatment of FGF1/CHIR99021 may increase pyruvate oxidation in ischemic myocardium. Because PDH converts pyruvate to acetyl-CoA which enters into the citric acid cycle (TCA cycle), we expect to find elevated levels of metabolites in the TCA cycle. However, our data showed a similarly increased abundance of certain intermediates in TCA cycle (citrate, cis-aconitate, isocitrate, oxoglutaric acid[a-ketoglutarate], and oxaloacetic acid) in the animals receiving NF_empty or NF_F + C at day 3 and day 7 post-MI compared to sham animals (Figure 3G). Considering that the TCA cycle is the central pathway of the three nutrients (carbohydrates, lipids, and

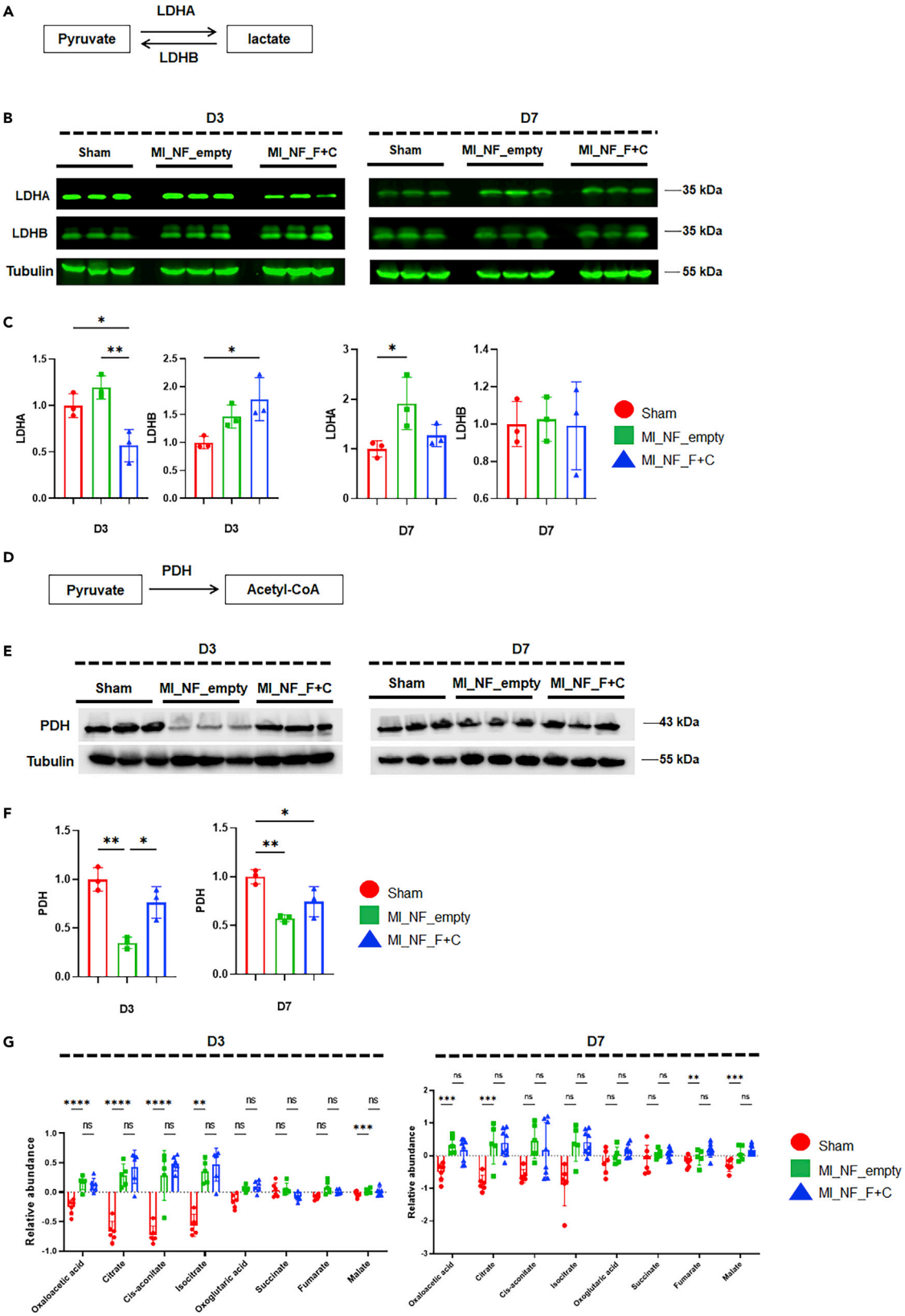
A
LDHA
Pyruvate
lactate
LDHB
B
D3
D7
Sham
MI_NF_empty
MI_NF_F+C
LDHA
LDHB
Tubulin
35 kDa
35 kDa
55 kDa
C
LDHA
LDHB
D3
D7
Sham
MI_NF_empty
MI_NF_F+C
D
PDH
Pyruvate
Acetyl-CoA
E
PDH
Tubulin
43 kDa
55 kDa
F
G
Relative abundance
Oxaloacetic acid
Citrate
Cis-aconitate
Isocitrate
Oxoglutaric acid
Succinate
Fumarate
Malate

Figure 3. Impact of FGF1/CHIR99021 on pyruvate oxidation and the TCA cycle in ischemic myocardium

Post-MI mice received intramyocardial injections of NF_empty or NF_F + C. Hearts were collected at day 3 and day 7 post-MI.

(A) Diagram of lactate metabolism.

(B) Heart tissues from infarct zone/border zone (IZ/BZ) of sham and post-MI mice were collected for Western blot analysis with antibodies against LDHA and LDHB.

(C) Densitometric signal quantitation of band intensity for LDHA and LDHB. Data were normalized to tubulin. (D) Diagram of the conversion from pyruvate to acetyl-CoA.

(E) Heart tissues from IZ/BZ of sham and post-MI mice were collected for Western blot analysis with antibodies against PDH.

(F) Densitometric signal quantitation of band intensity for PDH. Data were normalized to tubulin.

(G) Abundance of metabolites in TCA cycle 3- and 7-days post-MI. n = 3 per group for panel B, C, E and F. In panel G, on day 3, sham (n = 6), MI_NF_empty (n = 5), MI_NF_F + C (n = 6); on day 7, sham (n = 6), MI_NF_empty (n = 5), MI_NF_F + C (n = 8). Data in panel C, F and G are represented as mean+/−SD. *p < 0.05, **p < 0.01, ***p < 0.001, ****p < 0.0001. one-way ANOVA with Tukey's Honestly Significant Difference Test.

amino acids) in mitochondria, and acetyl-CoA is the hub that links the metabolism of carbohydrates, lipids, and amino acids, we speculate that other metabolism pathways (such as lipids and amino acids) may also be altered by myocardial ischemia and treatment of FGF1/CHIR99021.

FGF1/CHIR99021 has No impact on fatty acid oxidation in ischemic myocardium

To investigate whether the increase of intermediates in the TCA cycle in the animals receiving NF_empty or NF_F + C is because of augmented fatty acid metabolism that produces acetyl-CoA and enters the TCA cycle, fatty acid oxidation was evaluated. Our data showed that the abundance of palmitic acid, which is the most common saturated fatty acid, was reduced in the post-MI animals receiving NF_empty compared with sham animals at day 3 and day 7 post-MI, and this trend was partially normalized in the animals of NF_F + C group (Figure 4A). Acetylcarnitine is a molecule that transports fatty acids into the mitochondrial matrix for oxidation. The conversion of carnitine to acylcarnitine by carnitine palmitoyltransferase 1 (CPT1) is an essential step for fatty acid oxidation. Our data showed that the abundance of carnitine remained unchanged in sham and the two treatment groups of animals at day 3 and day 7 post-MI; however, acetylcarnitine was significantly reduced in the post-MI animals receiving NF_empty or NF_F + C compared with sham animals at day 3, and this trend was normalized at day 7 where no difference was found between post-MI and sham animals (Figure 4B). Acetyl-coenzyme A carboxylase (ACC) is a key enzyme in the biosynthesis of fatty acids that catalyzes the carboxylation of acetyl-CoA to malonyl-CoA, which subsequently inhibits the activity of CPT1, thus preventing fatty acids oxidation in mitochondria (Figure 4C). Phosphorylation by AMP-activated protein kinase at Ser79 inhibits the enzymatic activity of ACC. We performed Western blotting to examine the expression and phosphorylation of ACC. Our data showed that myocardial ischemia similarly inhibited the phosphorylation of ACC in the animals receiving NF_empty or NF_F + C compared to sham animals at day 3 and day 7 post-MI (Figures 4D and 4E). Taken together, these data suggest that the treatment of FGF1/CHIR990021 has no significant impact on ischemia-induced inhibition of fatty acid oxidation.

FGF1/CHIR99021 reduces BCAA accumulation in ischemic myocardium

Besides glucose and fatty acids, amino acids contribute to metabolism in ischemic myocardium (Drake et al., 2012; Lopaschuk et al., 2021). Analysis of metabolites in amino acid metabolism showed that 3 days of MI resulted in increased abundance of 15 different amino acids including ketogenic (leucine, lysine), glucogenic amino acids (alanine, aspartate, glutamic acid, proline, asparagine, glutamine, serine, and valine), and both ketogenic and glucogenic amino acids (isoleucine, phenylalanine, threonine, and tyrosine) except for methionine, arginine, and tryptophan (Figure 5A). These are also proteinogenic amino acids. It was reported that MI stimulates proteolysis and autophagy, thereby increasing the abundance of intracellular amino acids (Roczkowsky et al., 2020; Chan et al., 2019; Takagi et al., 2007; Matsui et al., 2007, 2008). However, hypertrophic growth of the myocardium in post-MI hearts is typically associated with highly active protein synthesis which exceeds protein degradation (Catalucci et al., 2008). Aromatic amino acids (phenylalanine, tryptophan, and tyrosine) are not metabolized in the heart. Therefore, these amino acids were used as markers for protein turnover (Drake et al., 2012). The abundance of phenylalanine and tyrosine increased at day 3 and day 7 post-MI, whereas the abundance of tryptophan remained unchanged at day 3 and increased at day 7 (Figure 5A). Because the ischemic heart is associated with impaired energy supply, the increased abundance of phenylalanine and tyrosine likely implicates elevated protein degradation.

It was reported that accumulation of BCAAs (leucine, isoleucine, and valine) contributes to ischemia-induced myocardial injury (Li et al., 2017, 2020; Uddin et al., 2019). Our data revealed the increased

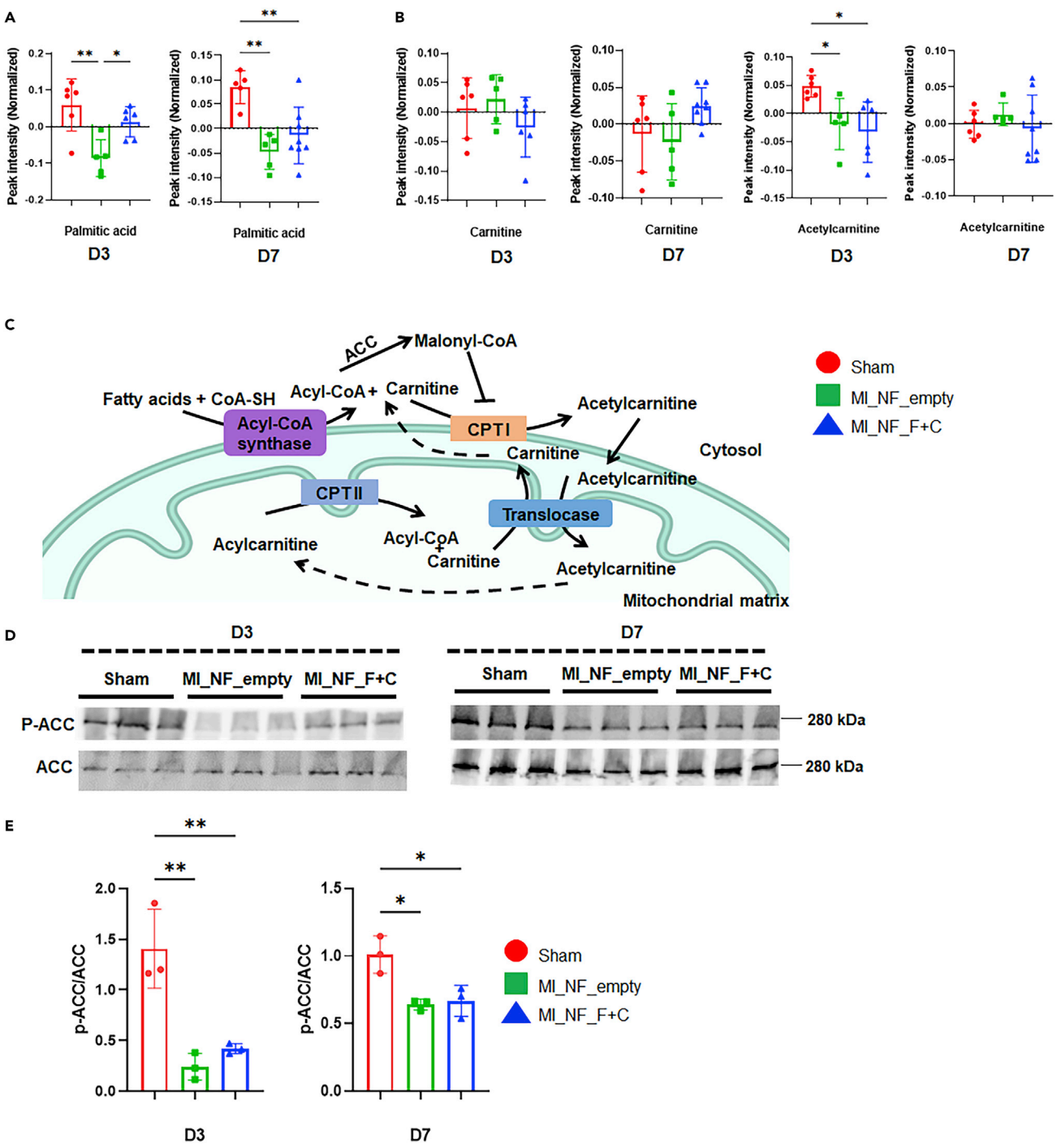

Figure 4. Impact of FGF1/CHIR99021 on fatty acid metabolism in ischemic myocardium

Post-MI mice received intramyocardial injections of NF_empty or NF_F + C. Hearts were collected at 3- and 7-days post-MI.

(A and B) Abundance of palmitic acid (A), carnitine, and acetylcarnitine (B) in infarct zone/border zone (IZ/BZ) myocardium at day 3 and day 7 post-MI.

(C) Diagram of fatty acid oxidation in mitochondria.

(D) Heart tissues from IZ/BZ of sham and post-MI mice were collected for Western blot analysis with antibodies against ACC and p-ACC.

(E) Densitometric signal quantitation of band intensity of p-ACC and total ACC and data were presented as the ratio of p-ACC to ACC. In panel A and B, for day 3, sham (n = 6), MI_NF_empty (n = 5), MI_NF_F + C (n = 6); for day 7, Sham (n = 6), MI_NF_empty (n = 5), MI_NF_F + C (n = 8). In panel D and E, n = 3 per group. Data in panel A, B and E are represented as mean+/−SD.*$p < 0.05$, **$p < 0.01$, one-way ANOVA with Tukey's Honestly Significant Difference Test.

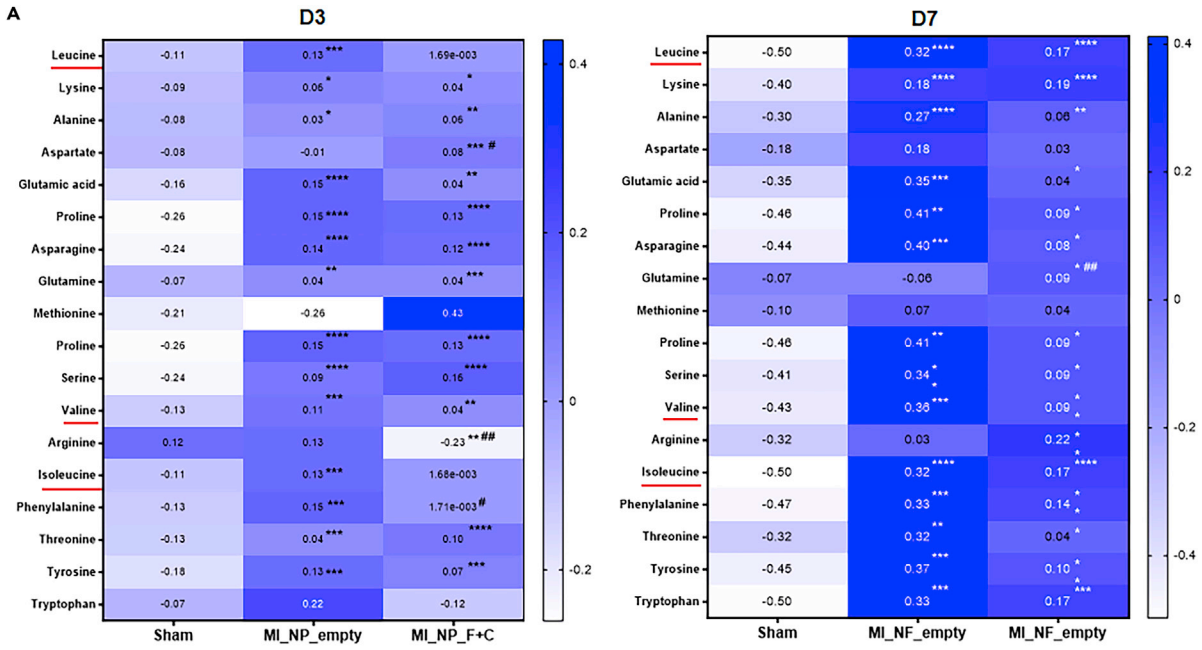
A
D3
D7
Leucine
Lysine
Alanine
Aspartate
Glutamic acid
Proline
Asparagine
Glutamine
Methionine
Proline
Serine
Valine
Arginine
Isoleucine
Phenylalanine
Threonine
Tyrosine
Tryptophan
Sham
MI_NP_empty
MI_NP_F+C
MI_NF_empty
MI_NF_empty
0.4
0.2
0
-0.2
-0.4

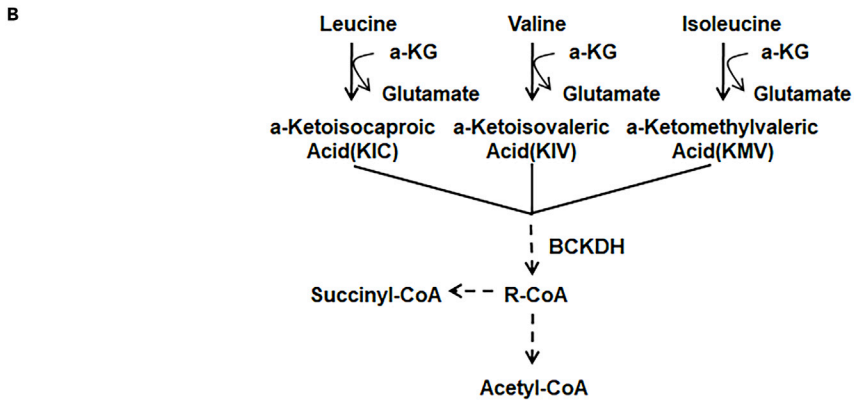
B
Leucine
Valine
Isoleucine
a-KG
Glutamate
a-Ketoisocaproic Acid(KIC)
a-Ketoisovaleric Acid(KIV)
a-Ketomethylvaleric Acid(KMV)
BCKDH
Succinyl-CoA
R-CoA
Acetyl-CoA

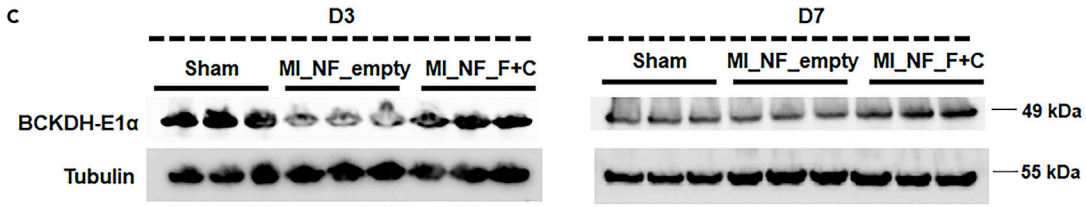
C
D3
D7
Sham
MI_NF_empty
MI_NF_F+C
BCKDH-E1α
Tubulin
49 kDa
55 kDa

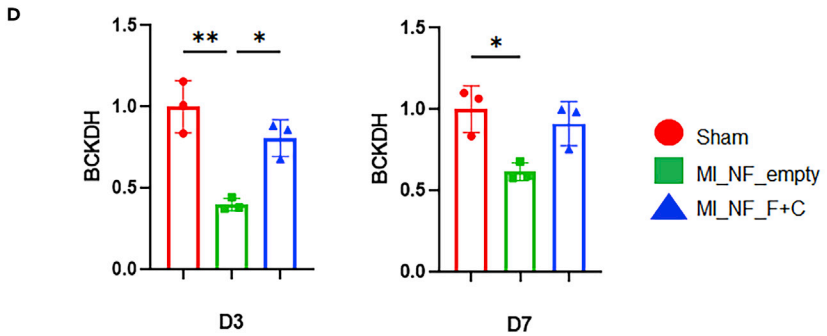
D
BCKDH
D3
D7
Sham
MI_NF_empty
MI_NF_F+C

Figure 5. Impact of FGF1/CHIR99021 on amino acids metabolism in ischemic myocardium

(A) Heart tissues from infarct zone/border zone (IZ/BZ) of sham and post-MI mice were collected for LC-MS/MS analysis. The heatmap of the abundance of amino acids in LC-MS/MS analysis was shown. For day 3, sham (n = 6), MI_NF_empty (n = 5), MI_NF_F + C (n = 6); for day 7, sham (n = 6), MI_NF_empty (n = 5), MI_NF_F + C (n = 8). Data are represented as mean. *p < 0.05, **p < 0.01, ***p < 0.001, ****p < 0.0001 compared with sham group, #p < 0.05, ##p < 0.01, ###p < 0.001, ####p < 0.0001 compared with MI_NF_empty group, one-way ANOVA with Tukey's Honestly Significant Difference Test.

(B) Diagram of branched amino acid metabolism.

(C) Western blot analysis with antibodies against BCKDH-E1α.

(D) Densitometric signal quantitation of band intensity for BCKDH-E1α. Data were normalized to tubulin, n = 3 per group for panel C and D, data in panel D are represented as mean+/−SD. *p < 0.05, **p < 0.01, one-way ANOVA with Tukey's Honestly Significant Difference Test.

abundance of BCAAs at day 3 post-MI, which was reduced by the treatment of FGF1/CHIR99021 (Figure 5A). At day 7 post-MI, though the treatment of FGF1/HIR99021 also showed the tendency to reduce BCAAs, the effects failed to reach a statistically significant level. BCAAs can be catalyzed by branched-chain amino acid aminotransferase (BCAT) isozymes (BCATm and BCATc), which forms Branched-chain α-keto acids (BCKAs) including α-ketoisocaproate (ketoleucine, KIC), α-keto-β-methylvalerate (ketoisoleucine, KMV), and α-ketoisovalerate (ketovaline, KIV) (Rietman et al., 2016; Islam et al., 2010; Cole et al., 2012). BCKAs are subsequently catalyzed by branched-chain alpha-keto acid dehydrogenase (BCKDH) complexes for oxidative decarboxylation and the synthesis of acetyl-CoA which enters the TCA cycle (Figure 5B). Branched-chain α-keto acid decarboxylase E1 subunit (BCKDH-E1) is one of three enzymatic components in the BCKDH complex (Li et al., 2017). To understand the molecular mechanisms of how FGF1/CHIR99021 inhibits BCAA accumulation, we performed Western blotting to determine the expression of the BCKDH complex. Our data showed that ischemia inhibited the expression of BCKDH-E1α, and the treatment of FGF1/CHIR99021 partially reverted this inhibition (Figures 5C and 5D). Taken together, these data suggest that FGF1/CHIR99021 inhibits ischemia-induced BCAA accumulation.

Metabolic profile in remote zone myocardium 3 and 7 Days Post-MI

Comparisons of the abundance of metabolites of remote zone myocardium of the three groups of animals at day 3 post-MI identified only one metabolite in carbohydrate metabolism (glycerate 3-phosphate) (Figure 6A) and two metabolites in lipid metabolism (myristic acid, hexanoic acid) (Figure 6B) with significant changes. The abundances of myristic acid and hexanoic acid were increased in remote zone myocardium of animals receiving NF_F + C compared with sham animals or animals receiving NF_empty (Figure 6B). Comparisons of the abundance of metabolites of remote zone myocardium of the three groups of animals also identified that 7 metabolites in the amino acid metabolic pathways (2-aminoadipic acid, 2-aminobutyric acid, methylguanidine, adenosyl-L-homocysteine, ketoleucine, pipecolinic acid, and creatinine) showed significantly changed abundance at day 3 (Figure 6C). NF_F + C treatment reduced the content of methylguanidine and creatinine, and increased the content of adenosyl-L-homocysteine, ketoleucine, and pipecolinic acid compared with NF_empty group. 2-aminoadipic acid and pipecolinic acid are the intermediate products in lysine metabolism (Lee et al., 2019; Chang, 1982). 2-aminobutyric acid and adenosyl-L-homocysteine are byproducts in the cysteine biosynthesis pathway. Methylguanidine and creatinine are the intermediates of creatine degradation. The abundance of 1-methyladenosine was increased in the hearts of post-MI mice receiving NF_F + C compared with sham and post-MI animals receiving NF_empty. The abundance of acetylcholine, a neurotransmitter, was reduced in both groups of MI mice compared with sham mice (Figure 6D). Comparisons of the abundance of metabolites of remote zone myocardium of the three groups of animals at 7 days post-MI identified only one metabolite (glutamic acid) with significant changes (Figure 6E). Taken together, these data suggest that there is no significant difference in the remote zone myocardium of post-MI animals as compared to sham animals.

DISCUSSION

Prolonged myocardial ischemia, such as MI, induces massive cardiomyocyte cell death (Thygesen et al., 2018). Cardiomyocyte death first appears in the subendocardial myocardium. Prolonged myocardial ischemia activates a "wavefront" of cardiomyocyte death that extends from the subendocardium to the subepicardium. This process continues for several days (Reimer et al., 1983). We recently reported that intramyocardial injection of NF_F + C protects against ischemia-induced cardiomyocyte death and improves heart function in post-MI mice and pigs (Fan et al., 2020a). Mechanisms underlying these cardioprotective effects have not been fully understood. Correction of metabolic disorder has been shown to confer cardioprotection against ischemia and reperfusion injuries (Jaswal et al., 2011). Therefore, we aimed to investigate whether improved myocardial metabolism contributes to FGF1 and CHIR99021-mediated

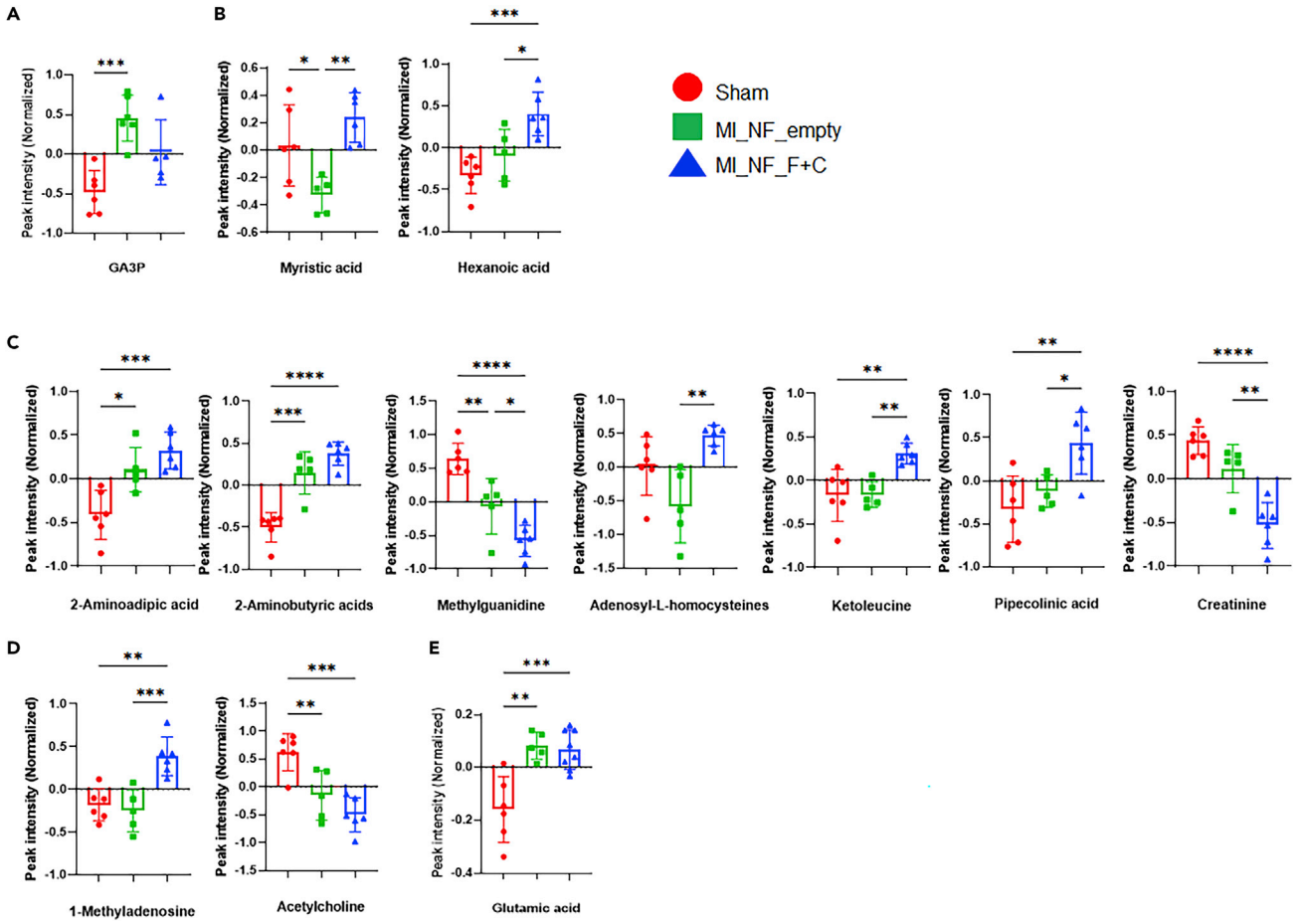

Figure 6. Metabolites profile in remote zone (RZ) myocardium of post-MI mice

Heart tissues from the RZ (upper part of left ventricle) myocardium were collected for LC-MS/MS analysis.

(A–D) Metabolite profile in remote zone myocardium at day 3 post-MI was shown, including metabolites in carbohydrate metabolic (glycerate 3-phosphate) (A), in the lipid metabolism (B), and in amino acid metabolism (2-aminoadipic acid, 2-aminobutyric acid, methylguanidine, adenosyl-L-homocysteine, ketoleucine, pipecolinic acid, and creatinine) (C). The abundance of 1-methyladenosine and acetylcholine (D).

(E) Metabolite prolife in remote zone myocardium at day 7 post-MI. In panel A-D, sham (n = 6), MI_NF_empty (n = 5), MI_NF_F + C (n = 6). In panel E, sham (n = 6), MI_NF_empty (n = 5), MI_NF_F + C (n = 8). Data in panel A-D are represented as mean +/− SD. *p < 0.05, **p < 0.01, ***p < 0.001, ****p < 0.0001, one-way ANOVA with Tukey's Honestly Significant Difference Test.

cardioprotection in post-MI animals. Our data indicated that treatment of FGF1 and CHIR99021 improves the capability of ischemic myocardium to generate energy via glycolysis and prevents BCAAs accumulation at the early stage post-MI (i.e., within the first 7 days).

The mammalian hearts require a high rate of ATP production continuously to maintain contractile function, basal metabolic processes, and ion homeostasis. In physiological conditions, most of ATP in the heart is produced from oxidation of fatty acids (>70%), and the rest of ATP is produced from the metabolism of glucose, lactic acid, and ketone bodies (Lopaschuk et al., 2010). Free fatty acids enter cardiomyocytes by passive diffusion or protein carrier-mediated pathways including fatty acid translocase (FAT)/CD36 (Gimeno et al., 2003). Myocardial ischemia is associated with insufficient oxygen supply which significantly limits cardiomyocytes' capacity to break down fatty acids. In response to ischemia, FAT/CD36 shifts away from the sarcolemma to prevent intramyocardial lipid accumulation, and this shift results in reducing fatty acid oxidation (Heather et al., 2013). Pharmacological activation of peroxisome proliferator-activated receptor-α (PPAR-α) increases fatty acid uptake, causes myocardial lipotoxicity, and exacerbates cardiac dysfunction in ischemic myocardium (Dewald et al., 2005). Cardiomyocyte-specific PPAR-α overexpression leads to cardiomyocyte death with deteriorated cardiac function after ischemia and reperfusion (Duerr et al., 2014). On the other hand, reducing fatty acid β-oxidation by inhibiting malonyl coenzyme A

decarboxylase protects the heart from ischemia injury via stimulating glucose oxidation and reducing lactic acid production, suggesting that reducing fatty acid oxidation and/or increasing glycolysis are cardioprotective in ischemic myocardium (Dyck et al., 2004). In the current study, the abundance of palmitic acid and/or acetylcarnitine is reduced in the ischemic hearts regardless of the treatment of FGF1 and CHIR99021 (Figures 4A and 4B), which is accompanied by decreased phosphorylation of ACC (Figures 4D and 4E) at day 3 and day 7 post-MI. These data suggested FGF1 and CHIR99021 have no impact on ischemia-induced inhibition of fatty acid oxidation in post-MI hearts.

Reduced fatty acid oxidation in ischemic myocardium decreases cellular citrate, which stimulates glucose uptake through glucose transporters GLUT1 and GLUT4 (Tran and Wang, 2019). Fatty acid and glucose transporters translocate between the sarcolemma and intracellular compartments to regulate substrate metabolism. Myocardial ischemia induces the increased sarcolemma content of GLUT4 by 90%, which is associated with an 86% increase in glycolytic rate (Heather et al., 2013). GLUT4 knockout mice showed decreased myocardial glucose utilization, severe systolic and diastolic dysfunction, and accelerated ATP depletion during ischemia (Tian and Abel, 2001). In the current study, the abundance of glucose and mannose is increased in post-MI animals receiving NF_empty compared with sham animals, and NF_F + C further increases the abundance of these metabolites (Figure 2A). Expression of rate-limiting enzymes in the glycolysis pathway were induced by ischemia and the treatment of FGF1 and CHIR99021, suggesting that the increased abundance of these metabolites is likely because of an increased utilization of glucose (Figures 2C and 2D). However, we do not know if ischemia and these pharmacological treatments also increase the uptake of glucose and mannose from the environment. Although glycolysis produces ATP in ischemic myocardium, increased glycolysis can cause the accumulation of potentially harmful catabolic products such as lactic acid and protons, leading to acidosis and intracellular Na^+ and Ca^{2+} overload (Jaswal et al., 2011). In the current study, we found that treatment of FGF1/CHIR99021 increases glycolysis but prevents lactic acid accumulation at day 3 post-MI (Figure 2A). Treatment of FGF1/CHIR99021 also inhibits the expression of LDHA and promotes the expression of LDHB (Figures 3B and 3C), which leads to increased conversion of lactic acid to pyruvate and thus prevents accumulation of lactic acid during increased glycolysis in ischemic myocardium. FGF1/CHIR99021 also increases the expression of PDH, which may promote pyruvate to enter into the mitochondrial matrix to form acetyl-CoA after oxidative decarboxylation.

Amino acid metabolism accounts for only a small proportion of cardiac ATP production in normal hearts. However, in the condition of myocardial ischemia, proteolysis, and autophagy are induced which leads to the increased intracellular amino acid abundance (Roczkowsky et al., 2020; Chan et al., 2019; Takagi et al., 2007; Matsui et al., 2007, 2008). The increased amino acids can be an important fuel source during prolonged ischemia (Drake et al., 2012). In the current study, the abundance of most amino acids is increased in animals receiving either NF_empty or NF_F + C at day 3 and day 7 post-MI (Figure 5A), suggesting an active amino acid metabolism during post-MI left ventricular remodeling. Ischemia also interrupts the catabolic metabolism of BCAAs, leading to the increased abundance of BCAAs (Li et al., 2017, 2020). Chronic accumulation of BCAAs suppresses glucose metabolism and sensitizes the heart to ischemic injury (Li et al., 2017). Elevated BCAAs directly suppress respiration and induce superoxide production in isolated mitochondria (Sun et al., 2016). Further studies discovered that the BCAAs in cardiomyocytes selectively disrupt mitochondrial pyruvate utilization through inhibition of PDH activity. Instead of downregulating PDH expression or increasing E1α phosphorylation, BCAAs directly inhibit PDH activity through protein O-linked-N-acetylglucosamine (O-GlcNAc) modification (Li et al., 2017). Cardiac-specific deletion of BCAA aminotransferase ($BCATm^{-/-}$), which is responsible for converting BCAAs to branched-chain keto acids (BCKAs), leads to a reduction in cardiac BCKAs, increased BCAAs, and impaired BCAA oxidation. In addition, the hearts from $BCATm^{-/-}$ mice show a higher increase in glucose oxidation induced by insulin stimulation compared with WT mice. Perfusing isolated working hearts with high levels of BCKAs completely eliminates the increased rate of glucose oxidation induced by insulin stimulation and inactivating PDH, suggesting that BCKAs but not BCAAs inhibit glucose oxidation (Uddin et al., 2021). On the contrary, increased intracellular glucose leads to BCAA accumulation by downregulating KLF15 and inhibiting the expression of BCAA-degrading enzymes (Shao et al., 2018). Reducing the level of myocardial BCAAs has been shown to improve cardiac function and left ventricular remodeling post-MI (Wang et al., 2016). Promoting BCAA catabolism or normalizing glucose utilization by overexpressing GLUT1 in the hearts with impaired BCAA catabolism rescues metabolic and functional disorders (Li et al., 2017). These studies suggested that there is a negative feedback regulation between glucose oxidation and branched-chain

amino acid degradation, which inhibits each other. In the current study, ischemia increases abundances of BCAAs compared with sham groups, whereas FGF1/HIR99021 prevents the accumulation of BCAAs via promoting the expression of BCKDH-E1α (Figure 5C).

In conclusion, our data support the notion that FGF1/CHIR99021 confers cardioprotection in post-MI mice via improving glycolysis and preventing the accumulation of BCAAs in ischemic myocardium.

Limitations of the study

First, we aimed to examine the alterations in major metabolic pathways. Therefore, we used the targeted LC-MS/MS method that was developed and used in a growing number of biological studies (Qi et al., 2020; Shao et al., 2018; Davis et al., 2018; Li et al., 2017), mainly because of the fact that the metabolites in the detection panel can be easily mapped into and connected to metabolic pathways. We targeted ~300 metabolites selected from >35 metabolic pathways of biological significance, including glycolysis, TCA cycle, purine metabolism, and amino acid metabolism. However, with current metabolomic techniques in an untargeted approach, upward of ~5000 features can be scanned, which could give a comprehensive metabolomic profile. To examine broad metabolic changes, we will use untargeted metabolomics in future studies. Second, the metabolomic studies were performed at the whole heart instead of single-cell level. The metabolism of nonmyocytes may potentially confound the results, which will be evaluated in future studies. Third, we did not determine the potential impact of FGF1 and CHIR99021 on the uptake of fatty acids and glucose in the ischemic myocardium. We cannot exclude the potential contribution of increased glucose uptake to the cardioprotection of FGF1 and CHIR99021.

STAR★METHODS

Detailed methods are provided in the online version of this paper and include the following:

- KEY RESOURCES TABLE
- RESOURCE AVAILABILITY
  - Lead contact
  - Materials availability
  - Data and code availability
- EXPERIMENTAL MODEL AND SUBJECT DETAILS
  - Animal
- METHOD DETAILS
  - Nanofiber preparation and characterization
  - Animal surgery
  - Metabolic analysis of heart tissue using liquid chromatography-tandem mass spectrometry (LC-MS/MS)
  - Western Blot
- QUANTIFICATION AND STATISTICAL ANALYSES
  - Statistical analyses

SUPPLEMENTAL INFORMATION

Supplemental information can be found online at https://doi.org/10.1016/j.isci.2022.104447.

ACKNOWLEDGMENTS

This work is supported by NIH grant (R01HL142627) and AHA TPA Award (20TPA35490001) to W.Z., and NIH grant (R01ES030197) to H.G.

AUTHOR CONTRIBUTIONS

Study Design, B.X., F.L., H.G., and W.Z.; Performing Experiments, Data Collection, and Analysis, B.X., F.L., W.Z., Y.S., L.T., P.L., J.J., A.Y., D.L., J.X., H.G., and W.Z.; Manuscript Writing, B.X., F.L., Z.W., S.W., J.X., H.G., and W.Z.

DECLARATION OF INTERESTS

The authors declare no competing interests

Received: December 13, 2021
Revised: April 16, 2022
Accepted: May 18, 2022
Published: June 17, 2022

REFERENCES

Ahmad, F., Singh, A.P., Tomar, D., Rahmani, M., Zhang, Q., Woodgett, J.R., Tilley, D.G., Lal, H., and Force, T. (2019). Cardiomyocyte-GSK-3α promotes mPTP opening and heart failure in mice with chronic pressure overload. J. Mol. Cell Cardiol *130*, 65–75. https://doi.org/10.1016/j.yjmcc.2019.03.020.

Baxter, G.F., Hale, S.L., Miki, T., Kloner, R.A., Cohen, M.V., Downey, J.M., and Yellon, D.M. (2000). Adenosine A1 agonist at reperfusion trial (AART): results of a three-center, blinded, randomized, controlled experimental infarct study. Cardiovasc. Drugs Ther. *14*, 607–614. https://doi.org/10.1023/a:1007850527878.

Bergman, B.C., Tsvetkova, T., Lowes, B., and Wolfel, E.E. (2009). Myocardial glucose and lactate metabolism during rest and atrial pacing in humans. J. Physiol. *587*, 2087–2099. https://doi.org/10.1113/jphysiol.2008.168286.

Botker, H.E., Cabrera-Fuentes, H.A., Ruiz-Meana, M., Heusch, G., and Ovize, M. (2020). Translational issues for mitoprotective agents as adjunct to reperfusion therapy in patients with ST-segment elevation myocardial infarction. J. Cell Mol Med *24*, 2717–2729. https://doi.org/10.1111/jcmm.14953.

Brown, D.A., Perry, J.B., Allen, M.E., Sabbah, H.N., Stauffer, B.L., Shaikh, S.R., Cleland, J.G.F., Colucci, W.S., Butler, J., Voors, A.A., et al. (2017). Expert consensus document: mitochondrial function as a therapeutic target in heart failure. Nat. Rev. Cardiol. *14*, 238–250. https://doi.org/10.1038/nrcardio.2016.203.

Bulluck, H., Sirker, A., Loke, Y.K., Garcia-Dorado, D., and Hausenloy, D.J. (2016). Clinical benefit of adenosine as an adjunct to reperfusion in ST-elevation myocardial infarction patients: an updated meta-analysis of randomized controlled trials. Int. J. Cardiol. *202*, 228–237. https://doi.org/10.1016/j.ijcard.2015.09.005.

Catalucci, D., Latronico, M.V., Ellingsen, O., and Condorelli, G. (2008). Physiological myocardial hypertrophy: how and why? Front. Biosci. *13*, 312–324. https://doi.org/10.2741/2681.

Chan, B.Y.H., Roczkowsky, A., Cho, W.J., Poirier, M., Lee, T.Y.T., Mahmud, Z., and Schulz, R. (2019). Junctophilin-2 is a target of matrix metalloproteinase-2 in myocardial ischemia-reperfusion injury. Basic Res. Cardiol. *114*, 42. https://doi.org/10.1007/s00395-019-0749-7.

Chang, Y.F. (1982). Lysine metabolism in the human and the monkey: demonstration of pipecolic acid formation in the brain and other organs. Neurochem. Res. *7*, 577–588. https://doi.org/10.1007/bf00965124.

Cluntun, A.A., Badolia, R., Lettlova, S., Parnell, K.M., Shankar, T.S., Diakos, N.A., Olson, K.A., Taleb, I., Tatum, S.M., Berg, J.A., et al. (2021). The pyruvate-lactate axis modulates cardiac hypertrophy and heart failure. Cell Metab *33*, 629–648.e10. https://doi.org/10.1016/j.cmet.2020.12.003.

Cole, J.T., Sweatt, A.J., and Hutson, S.M. (2012). Expression of mitochondrial branched-chain aminotransferase and alpha-keto-acid dehydrogenase in rat brain: implications for neurotransmitter metabolism. Front. Neuroanat. *6*, 18. https://doi.org/10.3389/fnana.2012.00018.

Dai, C., Li, Q., May, H.I., Li, C., Zhang, G., Sharma, G., Sherry, A.D., Malloy, C.R., Khemtong, C., Zhang, Y., et al. (2020). Lactate dehydrogenase A governs cardiac hypertrophic growth in response to hemodynamic stress. Cell Rep *32*, 108087. https://doi.org/10.1016/j.celrep.2020.108087.

Davis, R.J., Gonen, M., Margineantu, D.H., Handeli, S., Swanger, J., Hoellerbauer, P., Paddison, P.J., Gu, H., Raftery, D., Grim, J.E., et al. (2018). Pan-cancer transcriptional signatures predictive of oncogenic mutations reveal that Fbw7 regulates cancer cell oxidative metabolism. Proc. Natl. Acad. Sci. U S A *115*, 5462–5467. https://doi.org/10.1073/pnas.1718338115.

Dewald, O., Sharma, S., Adrogue, J., Salazar, R., Duerr, G.D., Crapo, J.D., Entman, M.L., and Taegtmeyer, H. (2005). Downregulation of peroxisome proliferator-activated receptor-alpha gene expression in a mouse model of ischemic cardiomyopathy is dependent on reactive oxygen species and prevents lipotoxicity. Circulation *112*, 407–415. https://doi.org/10.1161/circulationaha.105.536318.

Drake, K.J., Sidorov, V.Y., Mcguinness, O.P., Wasserman, D.H., and Wikswo, J.P. (2012). Amino acids as metabolic substrates during cardiac ischemia. Exp. Biol. Med. *237*, 1369–1378. https://doi.org/10.1258/ebm.2012.012025.

Duerr, G.D., Heinemann, J.C., Arnoldi, V., Feisst, A., Kley, J., Ghanem, A., Welz, A., and Dewald, O. (2014). Cardiomyocyte specific peroxisome proliferator-activated receptor-alpha overexpression leads to irreversible damage in ischemic murine heart. Life Sci. *102*, 88–97. https://doi.org/10.1016/j.lfs.2014.03.019.

Dunaway, G.A. (1983). A review of animal phosphofructokinase isozymes with an emphasis on their physiological role. Mol. Cell Biochem *52*, 75–91. https://doi.org/10.1007/bf00230589.

Dyck, J.R., Cheng, J.F., Stanley, W.C., Barr, R., Chandler, M.P., Brown, S., Wallace, D., Arrhenius, T., Harmon, C., Yang, G., et al. (2004). Malonyl coenzyme a decarboxylase inhibition protects the ischemic heart by inhibiting fatty acid oxidation and stimulating glucose oxidation. Circ. Res. *94*. e78-84. https://doi.org/10.1161/01.res.0000129255.19569.8f.

Eghlimi, R., Shi, X., Hrovat, J., Xi, B., and Gu, H. (2020). Triple negative breast cancer detection using LC-MS/MS lipidomic profiling. J. Proteome Res. *19*, 2367–2378. https://doi.org/10.1021/acs.jproteome.0c00038.

Fan, C., Oduk, Y., Zhao, M., Lou, X., Tang, Y., Pretorius, D., Valarmathi, M.T., Walcott, G.P., Yang, J., Menasche, P., et al. (2020a). Myocardial protection by nanomaterials formulated with CHIR99021 and FGF1. JCI Insight *5*, e132796. https://doi.org/10.1172/jci.insight.132796.

Fan, C., Tang, Y., Zhao, M., Lou, X., Pretorius, D., Menasche, P., Zhu, W., and Zhang, J. (2020b). CHIR99021 and fibroblast growth factor 1 enhance the regenerative potency of human cardiac muscle patch after myocardial infarction in mice. J. Mol. Cell Cardiol. *141*, 1–10. https://doi.org/10.1016/j.yjmcc.2020.03.003.

Fernandes, P.M., Kinkead, J., Mcnae, I., Michels, P.A.M., and Walkinshaw, M.D. (2020). Biochemical and transcript level differences between the three human phosphofructokinases show optimisation of each isoform for specific metabolic niches. Biochem. J. *477*, 4425–4441. https://doi.org/10.1042/bcj20200656.

Forde, J.E., and Dale, T.C. (2007). Glycogen synthase kinase 3: a key regulator of cellular fate. Cell Mol Life Sci *64*, 1930–1944. https://doi.org/10.1007/s00018-007-7045-7.

Fritz, P.J. (1965). Rabbit muscle lactate dehydrogenase 5; a regulatory enzyme. Science *150*, 364–366. https://doi.org/10.1126/science.150.3694.364.

Gasser, E., Moutos, C.P., Downes, M., and Evans, R.M. (2017). FGF1 - a new weapon to control type 2 diabetes mellitus. Nat. Rev. Endocrinol. *13*, 599–609. https://doi.org/10.1038/nrendo.2017.78.

Ghaderi, S., Alidadiani, N., Dilaver, N., Heidari, H.R., Parvizi, R., Rahbarghazi, R., Soleimani-Rad, J., and Baradaran, B. (2017). Role of glycogen synthase kinase following myocardial infarction and ischemia-reperfusion. Apoptosis *22*, 887–897. https://doi.org/10.1007/s10495-017-1376-0.

Gimenez-Cassina, A., Lim, F., Cerrato, T., Palomo, G.M., and Diaz-Nido, J. (2009). Mitochondrial hexokinase II promotes neuronal survival and acts downstream of glycogen synthase kinase-3. J. Biol. Chem. *284*, 3001–3011. https://doi.org/10.1074/jbc.m808698200.

Gimeno, R.E., Ortegon, A.M., Patel, S., Punreddy, S., Ge, P., Sun, Y., Lodish, H.F., and Stahl, A. (2003). Characterization of a heart-specific fatty acid transport protein. J. Biol. Chem. *278*, 16039–16044. https://doi.org/10.1074/jbc.m211412200.

Halestrap, A.P., Wang, X., Poole, R.C., Jackson, V.N., and Price, N.T. (1997). Lactate transport in heart in relation to myocardial ischemia. Am. J. Cardiol. *80*, 17A–25A. https://doi.org/10.1016/s0002-9149(97)00454-2.

Hausenloy, D.J., and Yellon, D.M. (2013). Myocardial ischemia-reperfusion injury: a

neglected therapeutic target. J. Clin. Invest. *123*, 92–100. https://doi.org/10.1172/jci62874.

Heather, L.C., Pates, K.M., Atherton, H.J., Cole, M.A., Ball, D.R., Evans, R.D., Glatz, J.F., Luiken, J.J., Griffin, J.L., and Clarke, K. (2013). Differential translocation of the fatty acid transporter, FAT/CD36, and the glucose transporter, GLUT4, coordinates changes in cardiac substrate metabolism during ischemia and reperfusion. Circ. Heart Fail *6*, 1058–1066. https://doi.org/10.1161/circheartfailure.112.000342.

Heusch, G. (2020). Myocardial ischaemia-reperfusion injury and cardioprotection in perspective. Nat. Rev. Cardiol. *17*, 773–789. https://doi.org/10.1038/s41569-020-0403-y.

Honkoop, H., De Bakker, D.E., Aharonov, A., Kruse, F., Shakked, A., Nguyen, P.D., De Heus, C., Garric, L., Muraro, M.J., Shoffner, A., et al. (2019). Single-cell analysis uncovers that metabolic reprogramming by ErbB2 signaling is essential for cardiomyocyte proliferation in the regenerating heart. Elife *8*, e50163. https://doi.org/10.7554/elife.50163.

Huang, C., Liu, Y., Beenken, A., Jiang, L., Gao, X., Huang, Z., Hsu, A., Gross, G.J., Wang, Y.G., Mohammadi, M., and Schultz, J.E.J. (2017). A novel fibroblast growth factor-1 ligand with reduced heparin binding protects the heart against ischemia-reperfusion injury in the presence of heparin co-administration. Cardiovasc. Res. *113*, 1585–1602. https://doi.org/10.1093/cvr/cvx165.

Hui, S., Ghergurovich, J.M., Morscher, R.J., Jang, C., Teng, X., Lu, W., Esparza, L.A., Reya, T., Le, Z., Yanxiang Guo, J., et al. (2017). Glucose feeds the TCA cycle via circulating lactate. Nature *551*, 115–118. https://doi.org/10.1038/nature24057.

Islam, M.M., Nautiyal, M., Wynn, R.M., Mobley, J.A., Chuang, D.T., and Hutson, S.M. (2010). Branched-chain amino acid metabolon: interaction of glutamate dehydrogenase with the mitochondrial branched-chain aminotransferase (BCATm). J. Biol. Chem. *285*, 265–276. https://doi.org/10.1074/jbc.M109.048777.

Israelsen, W.J., and Vander Heiden, M.G. (2015). Pyruvate kinase: function, regulation and role in cancer. Semin. Cell Dev Biol *43*, 43–51. https://doi.org/10.1016/j.semcdb.2015.08.004.

Jasbi, P., Shi, X., Chu, P., Elliott, N., Hudson, H., Jones, D., Serrano, G., Chow, B., Beach, T.G., Liu, L., et al. (2021). Metabolic profiling of neocortical tissue discriminates alzheimer's disease from mild cognitive impairment, high pathology controls, and normal controls. J. Proteome Res. *20*, 4303–4317. https://doi.org/10.1021/acs.jproteome.1c00290.

Jaswal, J.S., Keung, W., Wang, W., Ussher, J.R., and Lopaschuk, G.D. (2011). Targeting fatty acid and carbohydrate oxidation–a novel therapeutic intervention in the ischemic and failing heart. Biochim. Biophys. Acta *1813*, 1333–1350. https://doi.org/10.1016/j.bbamcr.2011.01.015.

Jiang, J., Chen, G., Shuler, F.D., Wang, C.H., and Xie, J. (2015). Local sustained delivery of 25-hydroxyvitamin D3 for production of antimicrobial peptides. Pharm. Res. *32*, 2851–2862. https://doi.org/10.1007/s11095-015-1667-5.

Jiang, J., Zhang, Y., Indra, A.K., Ganguli-Indra, G., Le, M.N., Wang, H., Hollins, R.R., Reilly, D.A., Carlson, M.A., Gallo, R.L., et al. (2018). 1α,25-dihydroxyvitamin D_3-eluting nanofibrous dressings induce endogenous antimicrobial peptide expression. Nanomedicine *13*, 1417–1432. https://doi.org/10.2217/nnm-2018-0011.

Juhaszova, M., Zorov, D.B., Yaniv, Y., Nuss, H.B., Wang, S., and Sollott, S.J. (2009). Role of glycogen synthase kinase-3beta in cardioprotection. Circ. Res. *104*, 1240–1252. https://doi.org/10.1161/CIRCRESAHA.109.197996.

Kahn, A., Meienhofer, M.C., Cottreau, D., Lagrange, J.L., and Dreyfus, J.C. (1979). Phosphofructokinase (PFK) isozymes in man. I. Studies of adult human tissues. Hum. Genet. *48*, 93–108. https://doi.org/10.1007/bf00273280.

Karwi, Q.G., Uddin, G.M., Ho, K.L., and Lopaschuk, G.D. (2018). Loss of metabolic flexibility in the failing heart. Front. Cardiovasc. Med. *5*, 68. https://doi.org/10.3389/fcvm.2018.00068.

Kolwicz, S.C., Jr., Purohit, S., and Tian, R. (2013). Cardiac metabolism and its interactions with contraction, growth, and survival of cardiomyocytes. Circ. Res. *113*, 603–616. https://doi.org/10.1161/circresaha.113.302095.

Lee, H.J., Jang, H.B., Kim, W.H., Park, K.J., Kim, K.Y., Park, S.I., and Lee, H.J. (2019). 2-Aminoadipic acid (2-AAA) as a potential biomarker for insulin resistance in childhood obesity. Sci. Rep. *9*, 13610. https://doi.org/10.1038/s41598-019-49578-z.

Leite, T.C., Coelho, R.G., Silva, D.D., Coelho, W.S., Marinho-Carvalho, M.M., and Sola-Penna, M. (2011). Lactate downregulates the glycolytic enzymes hexokinase and phosphofructokinase in diverse tissues from mice. FEBS Lett. *585*, 92–98. https://doi.org/10.1016/j.febslet.2010.11.009.

Li, T., Zhang, Z., Kolwicz, S.C., Jr., Abell, L., Roe, N.D., Kim, M., Zhou, B., Cao, Y., Ritterhoff, J., Gu, H., et al. (2017). Defective branched-chain amino acid catabolism disrupts glucose metabolism and sensitizes the heart to ischemia-reperfusion injury. Cell Metab *25*, 374–385. https://doi.org/10.1016/j.cmet.2016.11.005.

Li, Y., Xiong, Z., Yan, W., Gao, E., Cheng, H., Wu, G., Liu, Y., Zhang, L., Li, C., Wang, S., et al. (2020). Branched chain amino acids exacerbate myocardial ischemia/reperfusion vulnerability via enhancing GCN2/ATF6/PPAR-alpha pathway-dependent fatty acid oxidation. Theranostics *10*, 5623–5640. https://doi.org/10.7150/thno.44836.

Linseman, D.A., Butts, B.D., Precht, T.A., Phelps, R.A., Le, S.S., Laessig, T.A., Bouchard, R.J., Florez-Mcclure, M.L., and Heidenreich, K.A. (2004). Glycogen synthase kinase-3 phosphorylates bax and promotes its mitochondrial localization during neuronal apoptosis. J. Neurosci. *24*, 9993–10002. https://doi.org/10.1523/jneurosci.2057-04.2004.

Liu, J., Chen, G., Liu, Z., Liu, S., Cai, Z., You, P., Ke, Y., Lai, L., Huang, Y., Gao, H., et al. (2018). Aberrant FGFR tyrosine kinase signaling enhances the warburg effect by reprogramming LDH isoform expression and activity in prostate cancer. Cancer Res. *78*, 4459–4470. https://doi.org/10.1158/0008-5472.can-17-3226.

Lopaschuk, G.D., Belke, D.D., Gamble, J., Toshiyuki, I., and Schonekess, B.O. (1994). Regulation of fatty acid oxidation in the mammalian heart in health and disease. Biochim. Biophys. Acta *1213*, 263–276. https://doi.org/10.1016/0005-2760(94)00082-4.

Lopaschuk, G.D., and Jaswal, J.S. (2010). Energy metabolic phenotype of the cardiomyocyte during development, differentiation, and postnatal maturation. J. Cardiovasc. Pharmacol. *56*, 130–140. https://doi.org/10.1097/fjc.0b013e3181e74a14.

Lopaschuk, G.D., Karwi, Q.G., Tian, R., Wende, A.R., and Abel, E.D. (2021). Cardiac energy metabolism in heart failure. Circ. Res. *128*, 1487–1513. https://doi.org/10.1161/circresaha.121.318241.

Lopaschuk, G.D., Ussher, J.R., Folmes, C.D.L., Jaswal, J.S., and Stanley, W.C. (2010). Myocardial fatty acid metabolism in health and disease. Physiol. Rev. *90*, 207–258. https://doi.org/10.1152/physrev.00015.2009.

Lowry, O.H., and Passonneau, J.V. (1964). The relationships between substrates and enzymes of glycolysis in brain. J. Biol. Chem. *239*, 31–42. https://doi.org/10.1016/s0021-9258(18)51741-5.

Magadum, A., Singh, N., Kurian, A.A., Munir, I., Mehmood, T., Brown, K., Sharkar, M.T.K., Chepurko, E., Sassi, Y., Oh, J.G., et al. (2020). Pkm2 regulates cardiomyocyte cell cycle and promotes cardiac regeneration. Circulation *141*, 1249–1265. https://doi.org/10.1161/circulationaha.119.043067.

Mandarino, L.J., Printz, R.L., Cusi, K.A., Kinchington, P., O'doherty, R.M., Osawa, H., Sewell, C., Consoli, A., Granner, D.K., and Defronzo, R.A. (1995). Regulation of hexokinase II and glycogen synthase mRNA, protein, and activity in human muscle. Am. J. Physiol. *269*, E701–E708. https://doi.org/10.1152/ajpendo.1995.269.4.e701.

Matsui, Y., Kyoi, S., Takagi, H., Hsu, C.P., Hariharan, N., Ago, T., Vatner, S.F., and Sadoshima, J. (2008). Molecular mechanisms and physiological significance of autophagy during myocardial ischemia and reperfusion. Autophagy *4*, 409–415. https://doi.org/10.4161/auto.5638.

Matsui, Y., Takagi, H., Qu, X., Abdellatif, M., Sakoda, H., Asano, T., Levine, B., and Sadoshima, J. (2007). Distinct roles of autophagy in the heart during ischemia and reperfusion: roles of AMP-activated protein kinase and Beclin 1 in mediating autophagy. Circ. Res. *100*, 914–922. https://doi.org/10.1161/01.res.0000261924.76669.36.

McCullagh, K.J., Poole, R.C., Halestrap, A.P., Tipton, K.F., O'brien, M., and Bonen, A. (1997). Chronic electrical stimulation increases MCT1 and lactate uptake in red and white skeletal muscle. Am. J. Physiol. *273*, E239–E246. https://doi.org/10.1152/ajpendo.1997.273.2.e239.

Miura, T., and Tanno, M. (2010). Mitochondria and GSK-3β in cardioprotection against

ischemia/reperfusion injury. Cardiovasc. Drugs Ther. *24*, 255–263. https://doi.org/10.1007/s10557-010-6234-z.

Mottet, D., Dumont, V., Deccache, Y., Demazy, C., Ninane, N., Raes, M., and Michiels, C. (2003). Regulation of hypoxia-inducible factor-1α protein level during hypoxic conditions by the phosphatidylinositol 3-kinase/akt/glycogen synthase kinase 3β pathway in HepG2 cells. J. Biol. Chem. *278*, 31277–31285. https://doi.org/10.1074/jbc.m300763200.

Nederlof, R., Eerbeek, O., Hollmann, M.W., Southworth, R., and Zuurbier, C.J. (2014). Targeting hexokinase II to mitochondria to modulate energy metabolism and reduce ischaemia-reperfusion injury in heart. Br. J. Pharmacol. *171*, 2067–2079. https://doi.org/10.1111/bph.12363.

Nowbar, A.N., Gitto, M., Howard, J.P., Francis, D.P., and Al-Lamee, R. (2019). Mortality from ischemic heart disease. Circ. Cardiovasc. Qual. Outcomes *12*, e005375. https://doi.org/10.1161/circoutcomes.118.005375.

Ong, S.G., Lee, W.H., Theodorou, L., Kodo, K., Lim, S.Y., Shukla, D.H., Briston, T., Kiriakidis, S., Ashcroft, M., Davidson, S.M., et al. (2014). HIF-1 reduces ischaemia-reperfusion injury in the heart by targeting the mitochondrial permeability transition pore. Cardiovasc. Res. *104*, 24–36. https://doi.org/10.1093/cvr/cvu172.

Palmen, M., Daemen, M.J., De Windt, L.J., Willems, J., Dassen, W.R., Heeneman, S., Zimmermann, R., Van Bilsen, M., and Doevendans, P.A. (2004). Fibroblast growth factor-1 improves cardiac functional recovery and enhances cell survival after ischemia and reperfusion. J. Am. Coll. Cardiol. *44*, 1113–1123. https://doi.org/10.1016/j.jacc.2004.05.067.

Pitkanen, J.P., Torma, A., Alff, S., Huopaniemi, L., Mattila, P., and Renkonen, R. (2004). Excess mannose limits the growth of phosphomannose isomerase PMI40 deletion strain of Saccharomyces cerevisiae. J. Biol. Chem. *279*, 55737–55743. https://doi.org/10.1074/jbc.m410619200.

Powers, C.J., Mcleskey, S.W., and Wellstein, A. (2000). Fibroblast growth factors, their receptors and signaling. Endocr. Relat. Cancer *7*, 165–197. https://doi.org/10.1677/erc.0.0070165.

Purich, D.L., and Fromm, H.J. (1971). The kinetics and regulation of rat brain hexokinase. J. Biol. Chem. *246*, 3456–3463. https://doi.org/10.1016/s0021-9258(18)62152-0.

Qi, G., Mi, Y., and Yin, F. (2020). Cellular specificity and inter-cellular coordination in the brain bioenergetic System: implications for aging and neurodegeneration. Front. Physiol. *10*, 1531. https://doi.org/10.3389/fphys.2019.01531.

Reimer, K.A., Jennings, R.B., and Tatum, A.H. (1983). Pathobiology of acute myocardial ischemia: metabolic, functional and ultrastructural studies. Am. J. Cardiol. *52*, 72A–81A. https://doi.org/10.1016/0002-9149(83)90180-7.

Rietman, A., Stanley, T.L., Clish, C., Mootha, V., Mensink, M., Grinspoon, S.K., and Makimura, H. (2016). Associations between plasma branched-chain amino acids, beta-aminoisobutyric acid and body composition. J. Nutr. Sci. *5*, e6. https://doi.org/10.1017/jns.2015.37.

Roczkowsky, A., Chan, B.Y.H., Lee, T.Y.T., Mahmud, Z., Hartley, B., Julien, O., Armanious, G., Young, H.S., and Schulz, R. (2020). Myocardial MMP-2 contributes to SERCA2a proteolysis during cardiac ischaemia-reperfusion injury. Cardiovasc. Res. *116*, 1021–1031. https://doi.org/10.1093/cvr/cvz207.

Rylatt, D.B., Aitken, A., Bilham, T., Condon, G.D., Embi, N., and Cohen, P. (1980). Glycogen synthase from rabbit skeletal muscle. Amino acid sequence at the sites phosphorylated by glycogen synthase kinase-3, and extension of the N-terminal sequence containing the site phosphorylated by phosphorylase kinase. Eur. J. Biochem. *107*, 529–537.

Sancar, G., Liu, S., Gasser, E., Alvarez, J.G., Moutos, C., Kim, K., Van Zutphen, T., Wang, Y., Huddy, T.F., Ross, B., et al. (2022). FGF1 and insulin control lipolysis by convergent pathways. Cell Metab *34*, 171–183.e6. https://doi.org/10.1016/j.cmet.2021.12.004.

Shao, D., Villet, O., Zhang, Z., Choi, S.W., Yan, J., Ritterhoff, J., Gu, H., Djukovic, D., Christodoulou, D., Kolwicz, S.C., Jr., et al. (2018). Glucose promotes cell growth by suppressing branched-chain amino acid degradation. Nat. Commun. *9*, 2935. https://doi.org/10.1038/s41467-018-05362-7.

Shi, X., Wang, S., Jasbi, P., Turner, C., Hrovat, J., Wei, Y., Liu, J., and Gu, H. (2019). Database-assisted globally optimized targeted mass spectrometry (dGOT-MS): broad and reliable metabolomics analysis with enhanced identification. Anal. Chem. *91*, 13737–13745. https://doi.org/10.1021/acs.analchem.9b03107.

Stanley, W.C., Recchia, F.A., and Lopaschuk, G.D. (2005). Myocardial substrate metabolism in the normal and failing heart. Physiol. Rev. *85*, 1093–1129. https://doi.org/10.1152/physrev.00006.2004.

Suh, J.M., Jonker, J.W., Ahmadian, M., Goetz, R., Lackey, D., Osborn, O., Huang, Z., Liu, W., Yoshihara, E., Van Dijk, T.H., et al. (2014). Endocrinization of FGF1 produces a neomorphic and potent insulin sensitizer. Nature *513*, 436–439. https://doi.org/10.1038/nature13540.

Suh, J.M., Jonker, J.W., Ahmadian, M., Goetz, R., Lackey, D., Osborn, O., Huang, Z., Liu, W., Yoshihara, E., Van Dijk, T.H., et al. (2015). Erratum: corrigendum: Endocrinization of FGF1 produces a neomorphic and potent insulin sensitizer. Nature *520*, 388. https://doi.org/10.1038/nature14304.

Sun, H., Olson, K.C., Gao, C., Prosdocimo, D.A., Zhou, M., Wang, Z., Jeyaraj, D., Youn, J.Y., Ren, S., Liu, Y., et al. (2016). Catabolic defect of branched-chain amino acids promotes heart failure. Circulation *133*, 2038–2049. https://doi.org/10.1161/CIRCULATIONAHA.115.020226.

Takagi, H., Matsui, Y., Hirotani, S., Sakoda, H., Asano, T., and Sadoshima, J. (2007). AMPK mediates autophagy during myocardial ischemia in vivo. Autophagy *3*, 405–407. https://doi.org/10.4161/auto.4281.

Thygesen, K., Alpert, J.S., Jaffe, A.S., Chaitman, B.R., Bax, J.J., Morrow, D.A., and White, H.D.; Executive Group on behalf of the Joint European Society of Cardiology ESC/American College of Cardiology ACC/American Heart Association AHA/World Heart Federation WHF Task Force for the Universal Definition of Myocardial Infarction (2018). Fourth universal definition of myocardial infarction (2018). Circulation *138*, e618–e651. https://doi.org/10.1161/CIR.0000000000000617.

Tian, R., and Abel, E.D. (2001). Responses of GLUT4-deficient hearts to ischemia underscore the importance of glycolysis. Circulation *103*, 2961–2966. https://doi.org/10.1161/01.cir.103.24.2961.

Tran, D.H., and Wang, Z.V. (2019). Glucose metabolism in cardiac hypertrophy and heart failure. J. Am. Heart Assoc. *8*, e012673. https://doi.org/10.1161/jaha.119.012673.

Uddin, G.M., Karwi, Q.G., Pherwani, S., Gopal, K., Wagg, C.S., Biswas, D., Atnasious, M., Wu, Y., Wu, G., Zhang, L., et al. (2021). Deletion of BCATm increases insulin-stimulated glucose oxidation in the heart. Metabolism *124*, 154871. https://doi.org/10.1016/j.metabol.2021.154871.

Uddin, G.M., Zhang, L., Shah, S., Fukushima, A., Wagg, C.S., Gopal, K., Al Batran, R., Pherwani, S., Ho, K.L., Boisvenue, J., et al. (2019). Impaired branched chain amino acid oxidation contributes to cardiac insulin resistance in heart failure. Cardiovasc. Diabetol. *18*, 86. https://doi.org/10.1186/s12933-019-0892-3.

Wang, J., Liu, B., Han, H., Yuan, Q., Xue, M., Xu, F., and Chen, Y. (2015). Acute hepatic insulin resistance contributes to hyperglycemia in rats following myocardial infarction. Mol. Med. *21*, 68–76. https://doi.org/10.2119/molmed.2014.00240.

Wang, W., Zhang, F., Xia, Y., Zhao, S., Yan, W., Wang, H., Lee, Y., Li, C., Zhang, L., Lian, K., et al. (2016). Defective branched chain amino acid catabolism contributes to cardiac dysfunction and remodeling following myocardial infarction. Am. J. Physiol. Heart Circ. Physiol. *311*, H1160–H1169. https://doi.org/10.1152/ajpheart.00114.2016.

Watcharasit, P., Bijur, G.N., Song, L., Zhu, J., Chen, X., and Jope, R.S. (2003). Glycogen synthase kinase-3β (GSK3β) binds to and promotes the actions of p53. J. Biol. Chem. *278*, 48872–48879. https://doi.org/10.1074/jbc.m305870200.

Watcharasit, P., Thiantanawat, A., and Satayavivad, J. (2008). GSK3 promotes arsenite-induced apoptosis via facilitation of mitochondria disruption. J. Appl. Toxicol. *28*, 466–474. https://doi.org/10.1002/jat.1296.

Xie, J., Blough, E.R., and Wang, C.H. (2012). Submicron bioactive glass tubes for bone tissue engineering. Acta Biomater. *8*, 811–819. https://doi.org/10.1016/j.actbio.2011.09.009.

Yang, C.D., Shen, Y., Lu, L., Ding, F.H., Yang, Z.K., Zhang, R.Y., Shen, W.F., Jin, W., and Wang, X.Q. (2019). Insulin resistance and dysglycemia are associated with left ventricular remodeling after myocardial infarction in non-diabetic patients. Cardiovasc. Diabetol. *18*, 100. https://doi.org/10.1186/s12933-019-0904-3.

Ying, L., Wang, L., Guo, K., Hou, Y., Li, N., Wang, S., Liu, X., Zhao, Q., Zhou, J., Zhao, L., et al. (2021). Paracrine FGFs target skeletal muscle to exert potent anti-hyperglycemic effects. Nat. Commun. *12*, 7256. https://doi.org/10.1038/s41467-021-27584-y.

York, J.W., Penney, D.G., Weeks, T.A., and Stagno, P.A. (1976). Lactate dehydrogenase changes following several cardiac hypertrophic stresses. J. Appl. Physiol. *40*, 923–926. https://doi.org/10.1152/jappl.1976.40.6.923.

Zdralevic, M., Marchiq, I., De Padua, M.M.C., Parks, S.K., and Pouyssegur, J. (2017). Metabolic plasiticy in cancers-distinct role of glycolytic enzymes GPI, LDHs or membrane transporters MCTs. Front. Oncol. *7*, 313. https://doi.org/10.3389/fonc.2017.00313.

Zhu, W., Zhao, M., Mattapally, S., Chen, S., and Zhang, J. (2018). CCND2 overexpression enhances the regenerative potency of human induced pluripotent stem cell-derived cardiomyocytes: remuscularization of injured ventricle. Circ. Res. *122*, 88–96. https://doi.org/10.1161/circresaha.117.311504.

STAR★METHODS

KEY RESOURCES TABLE

REAGENT or RESOURCE	SOURCE	IDENTIFIER
Antibodies		
LDHA	Thermo Fisher Scientific	PA5-27406, RRID: AB_2544882
LDHB	Thermo Fisher Scientific	14824-1-AP, RRID: AB_2917990
Pyruvate Dehydrogenase	Cell signaling technology	3205T, RRID: AB_2162926
Hexokinase I (C35C4)	Cell signaling technology	2024T, RRID: AB_2116996
Hexokinase II (C64G5)	Cell signaling technology	2867T, RRID: AB_2232946
PKM1 (D30G6)	Cell signaling technology	7067T, RRID: AB_2715534
PKM2 (D78A4)	Cell signaling technology	4053T, RRID: AB_1904096
PFKP (D4B2)	Cell signaling technology	8164T, RRID: AB_2713957
Acetyl-CoA Carboxylase (C83B10)	Cell signaling technology	3676T, RRID: AB_2219397
Phospho-Acetyl-CoA Carboxylase (Ser79)	Cell signaling technology	3661T, RRID: AB_330337
BCKDH-E1α (E4T3D)	Cell signaling technology	90198S, RRID: AB_2800155
α/β-Tubulin	Cell signaling technology	2148T, RRID: AB_2288042
Anti-rabbit IgG, HRP-linked Antibody	Cell signaling technology	7074P2, RRID: AB_2099233
IRDye® 800CW Donkey anti-Rabbit IgG Secondary Antibody	Licor	AB_2715510, RRID: AB_621848
Chemicals, peptides, and recombinant proteins		
FGF1	R&D	232-FA
CHIR99021	Tocris	4423
Critical commercial assays		
Human FGF-acidic Quantikine ELISA kit	R&D	DFA00B
BCA kit	Thermo Fisher Scientific	89900
SuperSignal™ West Pico PLUS Chemiluminescent Substrate	Thermofisher	34577
Deposited data		
LC-MS/MS data	Data Archiving and Networked Services (DANS)	https://doi.org/10.17632/v7kpn27c4t.1
Experimental models: Organisms/strains		
C57/B6 mice	Jackson Laboratory	000664
Software and algorithms		
Prism v9	GraphPad	N/A
Odyssey CLx Infrared Imaging System	LI-COR Biosciences	N/A
Image Studio Lite Quantification Software	Bio-Rad	N/A

RESOURCE AVAILABILITY

Lead contact

Further information and requests for resources and reagents should be directed to and will be fulfilled by the lead contact, Wuqiang Zhu (zhu.wuqiang@mayo.edu).

Materials availability

This study did not generate new unique reagents.

Data and code availability

Data reported in this paper will be shared by the lead contact upon request. LC-MS/MS data have been deposited at "Cardiac metabolism in mice treated with FGF1- and CHIR99021-loaded nanofibers", Mendeley Data, V1, https://doi.org/10.17632/5hxw582v9r.1 (https://data.mendeley.com/datasets/5hxw582v9r/1) and are publicly available. This paper does not report original code. Any additional information required to reanalyze the data reported in this paper is available from the lead contact upon request.

EXPERIMENTAL MODEL AND SUBJECT DETAILS

Animal

All animal protocols were approved by the Institutional Animal Care and Use Committee (IACUC) of the Mayo Clinic. All animal surgical procedures and euthanasia were performed based on approved IACUC protocol and in accordance with the National Institutes of Health Guide for the Care and Use of Laboratory Animals. C57/B_6 mice were purchased from Jackson Laboratory. All mice were housed in a temperature- and humidity-controlled room and maintained on a 12:12 light:dark cycle, with standard chow and water *ad libitum*. For MI surgery, half male and half female, 4–6 weeks, body weight 20–26 g, were randomly assigned to experimental groups. Adult male and female mice were placed in same cage for mating. The neonatal mice (3–5 days after birth) were used for isolating cardiomyocytes.

METHOD DETAILS

Nanofiber preparation and characterization

CHIR99021 nanofibers was prepared using an electrospinning setup similar to what we had reported before (Jiang et al., 2015, 2018). In brief, 1 g poly lactic-*co*-glycolic acid (PLGA) (50:50) was dissolved in dichloromethane (DCM) at a concentration of 10% (w/v). CHIR99021 (16 mg) was dissolved in 1 mL dimethyl sulfoxide (DMSO) and was then added into the PLGA solution. The mixed solution was pumped at a flow rate of 1 mL/h while a potential of 10.0 kV was applied between the spinneret (a 22-gauge needle) and a grounded collector located 12 cm apart from the spinneret. A rotating drum was used to collect membranes composed of random fibers with a rotating speed less than 100 rpm.

The co-axial electrospinning setup was used to encapsulate FGF1 in the core of FGF1-PLGA core−shell nanofibers following the protocol we previously reported (Xie et al., 2012). In brief, 1 g PLGA (50:50) was dissolved in DCM at a concentration of 10% (w/v) to form the polymer phase. To prepare FGF1-PLGA core−shell fibers, 2 mg of FGF1 was dissolved in 1 mL ddH_2O to form the aqueous phase. The polymer phase was pumped at a flow rate of 1.0 mL/h to the shell, and the aqueous phase was pumped at a flow rate of 0.1 mL/h to the core, while a potential of 10 kV was applied between the spinneret (a 22-gauge needle) and a grounded collector located 12 cm apart from the spinneret. A rotating drum was used to collect membranes composed of random fibers with a rotating speed less than 100 rpm. The obtained fiber samples were processed into short fibers using a 6775 freezer/mill cryogenic grinder. All of the nanofibers were sterilized by ethylene oxide gas prior to *in vitro* cell culture and *in vivo* animal study.

FGF1 and CHIR99021 release kinetics were characterized as we described before (Fan et al., 2020a). CHIR99021 release studies were performed by sampling the supernatant of PLGA-CHIR99021 short nanofiber suspensions up to 7 days and were analyzed by high-performance liquid chromatography (HPLC). Briefly, the drug release solution was prepared using PBS and 1% bovine serum albumin. The PLGA--CHIR99021 short nanofibers were suspended at a concentration of 1 mg/mL of drug release solution and incubated at 37°C with constant stirring. At different time points, suspensions were centrifuged and 1 mL supernatant was collected and replaced with the fresh PBS solution. Samples flowed through the column at 1.0 mL/min and with a mobile phase consisting of acetonitrile and 0.1% trifluoroacetic acid solution (V/V). Samples were analyzed at 281 nm using a UV detector. Meanwhile, Slide-A-Lyzer MINI Dialysis Devices, 20K MWCO (Thermo Fisher Scientific) were used to determine the release kinetics of FGF1-loaded PLGA short nanofibers. FGF1-loaded PLGA short nanofibers were suspended the in buffer (PBS with 0.1% BSA and 0.02% sodium azide) in 0.5 mL dialysis device. The device was placed into the conical tube containing 14 mL the buffer. The medium was incubated at 37°C under constant shaking. At each defined time points 150 ul medium was collected as sample and replaced. FGF1 concentrations were calculated with the Human FGF-acidic Quantikine ELISA kit (R&D Systems) according to manufacturer recommendations. The FGF1 and CHIR99021 release profiles were shown in Figure S3.

Animal surgery

The MI and sham operation were performed on mice using the protocols we described before (Fan et al., 2020a, 2020b). In brief, animals were anesthetized with 2–4% inhaled isoflurane throughout the surgical procedure. Animals were intubated. Thoracotomy was performed and infarction was surgically induced via permanent ligation of left anterior descending coronary artery. PLGA nanofiber segments formulated with FGF1 (200 ng per heart) and CHIR99021 (2400 ng per heart), designated as NF_F + C, were intramyocardially injected to three sites in the infarct area immediately after coronary artery ligation (Figure 1A). The patch containing empty PLGA nanofiber segments (without FGF1 and CHIR99021), designated as NF_empty, was used as the control. Buprenorphine SR Lab subcutaneous injection (0.4-1 mg/kg) was performed immediately after surgery and then every 72 h as needed. Animals were euthanized via inhaled carbon dioxide and secondary method to confirm euthanasia via cervical dislocation. The first cohort were euthanized at day 3 and the second cohort at day 7 post surgery. The animal hearts were harvested, the ventricles were isolated and cut at the coronal plane at 0.5 mm above the suture line (Figure 1B). The upper part represents non-infarction zone or remote zone, and the lower part represents infarction and border zones. Animal number for day 3 sham group (n = 6; 3 male and 3 female), MI_NF_empty group (n = 5; 3 male and 2 female), MI_NF_F + C group (n = 6; 3 male and 3 female). Animal number for day 7, sham group (n = 6; 3 male and 3 female), MI_NF_empty group (n = 5; 3 male and 2 female), MI_NF_F + C group (n = 8; 4 male and 4 female).

Metabolic analysis of heart tissue using liquid chromatography-tandem mass spectrometry (LC-MS/MS)

We implemented a pathway-specific LC-MS/MS method that can cover more than 300 metabolites from >35 metabolic pathways (Eghlimi et al., 2020; Shi et al., 2019; Jasbi et al., 2021). In brief, a small block of tissue (~20 mg) from each heart was utilized. The heart tissues were homogenized in 200 μL MeOH:PBS (4:1, v:v). The MeOH:PBS solution (800 μL) were then added to the lysate. The cell lysates were vortexed for 10 s and then stored at −20°C for 30 min. Samples were sonicated in an ice bath for 30 min and were spun down with a refrigerated centrifuge (4°C) for 10 min with a speed of 21,694 xg. A total of 800 μL supernatant was transferred to a new Eppendorf tube and vacuum dried. The pellets were then reconstituted with 150 μL solution containing 40% PBS and 60% acetonitrile before mass spectrometry (MS) analysis. A quality control (QC) sample was prepared by pooling all the study samples. Each sample was injected twice into the targeted LC-MS/MS system. One injection of 10 μL was for analysis with negative ionization mode. The other injection of 4 μL was used for analysis with positive ionization mode. Both chromatographic separations were performed in hydrophilic interaction chromatography mode on a Waters XBridge BEH Amide column (150 × 2.1 mm, 2.5 μm particle size). The flow rate was set as 0.3 mL/min. The auto-sampler temperature was set at 4°C. The column compartment was kept at 4°C. The mobile phase was composed of Solvents A (10 mM ammonium acetate, 10 mM ammonium hydroxide in a mixed solution containing 95% H_2O and 5% acetonitrile) and Solvents B (10 mM ammonium acetate, 10 mM ammonium hydroxide in a mixed solution containing 5% H_2O and 95% acetonitrile). After the initial isocratic elution for 1 min, the percentage of Solvent B was reduced to 40% (t = 11 min), and it was maintained at 40% for 4 min (t = 15 min). The mass spectrometer is equipped with an electrospray ionization source. Targeted data acquisition was performed in multiple-reaction-monitoring (MRM) mode. The extracted MRM peaks were integrated using Agilent MassHunter Quantitative Data Analysis.

Western Blot

A small piece (~100 mg) of left ventricular tissue from each mouse was isolated. Whole cell lysate was generated using the protocol we reported before (Zhu et al., 2018). Protein concentration was measured with a BCA kit (Thermo Fisher Scientific, cat# 89900). Samples were solubilized in sodium dodecyl sulfate (SDS)-polyacrylamide gel electrophoresis (PAGE) loading buffer for 5 min at 95°C and resolved on SDS–PAGE gels. After the electro-transferred from the gel to nitrocellulose membrane (Amersham), the primary antibodies were incubated at 4° for one night, and the secondary antibodies were incubated at RT for 1 h. Signal was visualized by Odyssey CLx Infrared Imaging System (LI-COR Biosciences) or Bio-rad ChemiDoc XRS + Chemiluminescence Imaging System. Western signal was digitized and quantitated using Image Studio Lite Quantification Software or ImageJ.

QUANTIFICATION AND STATISTICAL ANALYSES

Statistical analyses

The data obtained from LC-MS/MS assay were log10 transformed, mean-centered, and divided by the square root of standard deviation (SD) for each metabolite (Pareto-scaled) to approximate normal distribution. Data from all PCA and Variance Analysis (Figures 1C, 1D, 1E, and 1F) were processed for univariate statistical testing using one-way ANOVA with Fisher's Least Significance Difference Test in the Metaboanalyst 5.0 package to compare the relative concentrations of metabolites between cohorts. Data from all metabolites, as well as western blot experiments (Figure 2A, 2D, 3C, 3F, 3G, 4A, 4B, 4E 5D, and 6A–6E) were presented as Mean $\pm$ SD. Figure 5A was presented as heatmap with Mean. Statistics were analyzed using Graphpad Prism 9.0. Differences among three groups were evaluated by one-way ANOVA with Tukey's Honestly Significant Difference Test. $p < 0.05$ was considered statistically significant.